Article:
Douglas, KM orcid.org/0000-0002-3281-3685, Blitz, MA, Mangan, TP orcid.org/0000-0001-7053-5594 et al. (2 more authors) (2020) Kinetic Study of the Reactions PO + O2 and PO2 + O3 and Spectroscopy of the PO Radical. The Journal of Physical Chemistry A. ISSN 1089-5639

https://doi.org/10.1021/acs.jpca.0c06106

Kinetic Study of the Reactions PO + O_2 and PO_2 + O_3 and Spectroscopy of the PO Radical

Kevin M. Douglas[a*], Mark A. Blitz[a,b], Thomas P. Mangan[a], , Colin M. Western[c], John M.C. Plane[a*]

[a]*School of Chemistry, University of Leeds, Leeds, LS2 9JT, UK*

[b]*National Centre for Atmospheric Science (NCAS), University of Leeds, Leeds, LS2 9JT, UK*

[c]*School of Chemistry, University of Bristol, BS8 1TS, UK*

[*]*Corresponding authors emails: K.M.Douglas@leeds.ac.uk; J.M.C.Plane@leeds.ac.uk*

Abstract

The kinetics of the reactions of PO with O_2 and PO_2 with O_3 were studied at temperatures ranging from ~ 190 to 340 K, using a pulsed laser photolysis-laser induced fluorescence technique. For the reaction of PO + O_2 there is evidence of both a two- and three-body exit channel, producing PO_2 + O and PO_3, respectively. Potential energy surfaces of both the PO + O_2 and PO_2 + O_3 systems were calculated using electronic structure theory, and combined with RRKM calculations to explain the observed pressure and temperature dependences. For PO + O_2, at pressures typical of a planetary upper atmosphere where meteoric ablation of P will occur, the reaction is effectively pressure independent with a yield of PO_2 + O of > 99%; the rate coefficient can be expressed by: $\log_{10}(k, 120 - 500\ \text{K}, \text{cm}^3\ \text{molecule}^{-1}\ \text{s}^{-1}) = -13.915 + 2.470\log_{10}(T) - 0.5020(\log_{10}(T))^2$, with an uncertainty of ± 10 % over the experimental temperature range (191 – 339 K). With increasing pressure, the yield of PO_3 increases, reaching ~ 90% at a pressure of 1 atm and T = 300 K. For PO_2 + O_3, $k(188 - 339\ \text{K}) = 3.7 \times 10^{-11} \exp^{(-1131/T)}\ \text{cm}^3\ \text{molecule}^{-1}\ \text{s}^{-1}$, with an uncertainty of ± 26 % over the stated temperature range. Laser induced fluorescence spectra of PO over the wavelength range of 245 – 248 nm were collected and simulated using PGOPHER to obtain new spectroscopic constants for the ground and v = 1 vibrational levels of the $X^2\Pi$ and $A^2\Sigma^+$ states of PO.

1. Introduction

Phosphorus, P, is one of main biogenic elements, a group which, along with H, C, O, N, and S, are present in all known life forms. Compounds of phosphorus appear profusely in biological systems, where they are involved in many fundamental biological functions, including replication, information transfer, and metabolism.[1] Despite its biological importance, P is relatively scarce on a cosmic scale. With an elemental abundance of 3.4×10^{-7} relative to H in the Sun's atmosphere,[2] it is the least abundant of the main biogenic elements. Ortho-phosphate (oxidation state +5), is the dominant form of inorganic P at the Earth's surface. However, P(V) salts typically exhibit poor bioavailability due to their low water solubility, and low reactivity. Indeed, low concentrations of dissolved P make it a

limiting reaction in many ecosystems, as well as giving rise to the 'phosphorus problem' in the origin or life.[3-4] In contrast, the salts of more reduced forms of P (oxidation state ≤ +3) are far more soluble and reactive, and thus have improved bioavailability.

One possible source of these reduced forms of P is from extra-terrestrial material that fell to Earth during the heavy bombardment period. A study by Pasek[5] demonstrated how phosphides, delivered directly to the surface of the Earth in iron nickel meteorites, can be processed by aqueous phase chemistry to form several prebiotic P species. However, of the total annual mass influx of exogenous material entering the Earth's atmosphere, iron nickel meteorites only account for ~ 1%, with interplanetary dust particles (IDPs) accounting for the other 99 %.[6] An alternative entry route for reduced forms of exogenous P is the atmospheric processing of P that ablates in the upper atmosphere. In two previous publications we have demonstrated that the meteoric ablation of IDPs is a significant source of atmospheric P, PO, and PO_2 to the terrestrial planets,[7] and how any P atoms will be rapidly oxidised to PO.[8] Continued atmospheric processing of PO and PO_2 will then result in a variety of compounds in which P may exist in different oxidation states, due to the presence of both oxidizing and reducing agents in these atmospheres. Figure 1 shows a schematic diagram of the likely chemistry of meteor-ablated P species. This scheme was constructed by performing high-level electronic structure calculations (at the CBS-QB3 level of theory[9]) of P species reacting with atmospherically relevant species to determine energetically viable reaction pathways. Following initial oxidation of P and PO to PO_2 (*via* reactions R1 and R2a), there appear to be two main channels: the formation of phosphoric acid (H_3PO_4) *via* the species $HOPO_2$ (reactions R6 and R7), or the formation of the bioavailable compound phosphonic acid (H_3PO_3) *via* HPO_2 (reactions R8 and R9):

	$\Delta H^{\circ}_{(0\,K)}$ (kJ mol^{-1})	
$P(^4S) + O_2 \rightarrow PO + O$	- 100	(R1)
$PO + O_2 \rightarrow PO_2 + O$	- 12	(R2a)
$PO + O_2 (+M) \rightarrow PO_3 (+M)$	- 416	(R2b)
$PO_2 + O_3 \rightarrow PO_3 + O_2$	- 305	(R3)
$PO_3 + H \rightarrow PO_2 + OH$	- 22	(R4)
$PO_3 + O \rightarrow PO_2 + O_2$	- 93	(R5)
$PO_2 + OH (+ M) \rightarrow HOPO_2 (+ M)$	- 441	(R6)
$HOPO_2 + H_2O (+ M) \rightarrow H_3PO_4 (+ M)$	- 188	(R7)
$PO_2 + H (+ M) \rightarrow HPO_2 (+ M)$	- 333	(R8)
$HPO_2 + H_2O (+ M) \rightarrow H_3PO_3 (+ M)$	- 173	(R9)

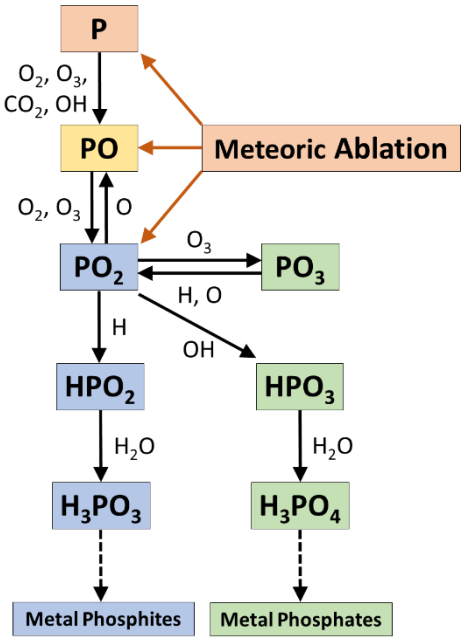

Figure 1. Proposed reaction scheme for the neutral chemistry of P in the upper atmosphere of a terrestrial planet.

At present, only two reactions from this scheme have been previously investigated (R1 and R2). The temperature dependence of reaction R1 was reported in a previous publication from this group, in which the reactions of both ground and excited state P atoms with atmospherically relevant species were investigated.[8] Prior to this, only room temperature determinations of the rate of R1 were available, and the literature rate coefficients reported disagreed by over an order of magnitude [10-13]. For reaction R2 there is similar disagreement in the literature, with four previous room temperature rate coefficients reported. Two of the studies [14-15] put the rate at around 2×10^{-13} cm^3 molecule^{-1} s^{-1}, while the other two studies [16-17] put the rate at around 60 times faster than this, with a value of ~ 1.3×10^{-11} cm^3 molecule^{-1} s^{-1}. This poor characterization of the gas-phase chemistry of phosphorus is not only of consequence to planetary atmospheres, as P-bearing compounds, including PO [18-20], have been detected in a range of astrochemical environments. Many current chemical models are using the isovalence between nitrogen and phosphorus to derive chemical rates for P-bearing species, the validity of which is questionable as these models tend to significantly underpredict the observed abundances of PO. Indeed, modelled and observed abundances of PO in a stellar outflow, in which PO is formed from the reaction of P + OH → PO + H, disagree by greater than 3 orders-of-magnitude.[21] Understanding the oxidation chemistry of elemental phosphorus and its oxides is also of importance to combustion chemistry, as phosphorus-containing compounds may be useful as potential fire suppression agents.[22-24] An understanding of the combustion of organophosphate compounds is of particular importance in the destruction of chemical warfare agents.[25-26]

The PO radical has been studied extensively by spectroscopic methods, with a brief history of the experimental work given by Moussaoui *et al.*[27]. Studies investigating the $A^2\Sigma^+ \leftarrow X\,^2\Pi$ transition include those by Coquart *et al.*[28], Sausa *et al.*[17], and Wong *et al.*[29]. There

have also been numerous theoretical studies, with a good overview of these given by Liu *et al.*[30]. These theoretical studies have provided potential energy curves for the ground and many excited states of PO and also transition dipole moments for electric dipole transitions. However, as the $A^2\Sigma^+$ state is a low-lying Rydberg state, it is completely missed by the *ab initio* calculations employed in the majority of these theoretical studies, making the available literature on the $A^2\Sigma^+$ state rather sparse.[31]

In this paper, we present results from the second part of our investigation into the reactions of meteor-ablated phosphorus, reporting temperature-dependent rate coefficients for reactions R2 and R3. Rate coefficients were determined using a pulsed laser photolysis-laser induced fluorescence (PLP-LIF) technique, which is described in Section 2. Using the same experimental setup, LIF spectra of PO over the wavelength range of 245 – 248 nm were also collected. These spectra are then assigned and new spectroscopic constants for the $X\,^2\Pi$ and $A^2\Sigma^+$ states of PO reported.

2. Experimental Procedure

2.1 Reaction kinetics

The experimental apparatus employed in this study has been discussed in detail in recent publications,[8, 32-34] so only a brief synopsis is given here. All experiments were carried out in a slow flow reaction cell, using a PLP-LIF technique, with detection of either PO or PO_2 radicals. The reaction cell consists of a cylindrical stainless steel chamber with four orthogonal horizontal side arms, and a fifth vertical side arm. The chamber was enclosed in a thermally insulated container, which can be operated as a furnace or filled with dry ice, providing a temperature range from 190 – 800 K. Temperatures inside the reactor were monitored by a shielded K-type thermocouple inserted directly into the centre of the chamber. Radical precursors, reagents, and bath gases were introduced to the chamber *via* the 5 side arms, after being combined in a mixing manifold to ensure homogeneous mixing. Radical precursors were prepared as dilute mixtures of between 0.5 and 5 % in N_2 (total precursor concentrations in the cell were typically around 0.1 %). Flow rates were controlled using calibrated mass flow controllers (MKS instruments), with total flow rates ranging from 100 – 400 standard cm^{-3} min^{-1}. These flow rates were sufficient to ensure a fresh flow of gas through the interaction region for each photolysis laser pulse. The pressure inside the reaction chamber was measured by a calibrated capacitance manometer (Baratron MKS PR 4000), and controlled by a needle valve on the exit line to the pump. The photolysis and probe laser beams were introduced collinearly on opposite sides of the cell, and the fluorescence signal collected using a photomultiplier tube (PMT) (Electron Tubes, model 9816QB) mounted orthogonally to the laser beams. To increase the solid angle of collected fluorescence, a glass tube of ~1.5 cm diameter was positioned ~1 cm above the interaction region to act as a waveguide to transport the fluorescence light along the vertical side arm to the PMT.

For reaction R2, PO radicals were produced from the multiphoton dissociation of $POCl_3$ at 248 nm (R10). For reaction R3, PO_2 radicals were produced by the photolysis of either $POCl_3$ or PCl_3 at 248 nm, in the presence of O_3. O_3 was produced by passing a flow of

O_2 though a corona discharge in an ozonizer (Edwards, E28), with a typical conversion efficiency of ~ 2 %. O_3 concentrations were monitored downstream of the reactor, by either UV or green light absorption spectroscopy. UV absorption spectroscopy was carried out at 253.7 nm from a Hg Pen-ray lamp, using a 1 m absorption cell with a PMT (Hamamatsu Type H9306-13) fitted with a monochromator set at 257.3 nm (Minichrom, 300 μm slits). Green light absorption spectroscopy was carried out using a multipass Herriott cell,[35] with a total pass length of 1.38 m. Green light at 532 nm was produced using a solid state laser, and monitored using a photodiode detector (Thorlabs SM05PD3A) connected to digital oscilloscope (LeCroy, LT262). Ozone concentrations were determined using absorption cross sections taken from the MPI-Mainz Spectral Atlas[36] (1.16×10^{-17} cm^2 at 253.7 nm and 3.0×10^{-21} cm^2 at 532 nm). Corrections were made to the measured ozone concentrations to account for photolysis by the 248 nm photolysis laser in the reaction chamber. This was done by first determining the intensity of 248 nm light entering the reaction cell (as measured by a Gentec UP19-VR power meter) and reaching the interaction region, after accounting for loses due to windows and attenuation by O_3 in the 15 cm side-arm. Then, using the intensity of light reaching the interaction region, the number of photons of 248 nm light absorbed by O_3 over the 1 cm interaction region was calculated. Assuming that each photon of 248 nm light absorbed led to the photo-dissociation of one O_3 molecule,[37] the remaining concentration of O_3 in the interaction region could then be determined. In a typical experiment, at high ozone concentrations of ~ 6×10^{15} molecule cm^{-3}, around 10 % of the O_3 within the 1 cm^3 interaction region was removed, while at lower ozone concentrations of ~ 6×10^{14} molecule cm^{-3} around 20 % of the ozone was removed. To validate this method of correcting the ozone concentration, the reduction in the intensity of the 248 nm light due to absorption by O_3 as it passed through the entire cell was also calculated, and shown to be in good agreement with measured reductions in the 248 nm light intensity exiting the cell.

In all experiments, the 248 nm photolysis light was generated from a KrF excimer laser (Lambda Physik COMPEX 102). In experiments requiring multiphoton dissociation of the precursor, the excimer beam was loosely focused using a 50 cm focal length lens, with the focal point positioned approximately 10 cm beyond the centre of the reaction chamber, giving a beam cross-section in the interaction region of ~ 8 mm^2. The KrF laser fluence at the interaction region ranged from between 10 – 20 mJ cm^{-2} for experiments in which no focusing was required, and from between 270 – 650 mJ cm^{-2} for experiments in which focusing was required. PO and PO_2 radicals were observed by time-resolved LIF spectroscopy, using the frequency doubled output of a Nd:YAG pumped dye laser (a Quantel Q-smart 850 pumping a Sirah Cobra-Stretch with a BBO doubling crystal). PO($X^2\Pi$) was probed using the $A^2\Sigma^+$ ($v' = 0$) ← $X^2\Pi$ ($v'' = 0$) transition at ~ 246.3 nm.[17] The non-resonant (v',v'' 0,1) fluorescence at ~ 255.4 nm was collected using a PMT fitted with an appropriate filter (Laser2000 Brightline Bandpass filter, λ_{max} – 255 nm, fwhm – 8 nm), and recorded using a digital oscilloscope (LeCroy, LT262). PO_2 was probed using either the $B\ ^2B_1$ (2,7,0) ← X $^2A_1$ (0,0,0) transition at ~ 286.1 nm or the $B\ ^2B_1$ (4,2,0) ← X $^2A_1$ (0,0,0) at 287.0 nm, and the non-resonant fluorescence at $\lambda > 350$ nm discriminated using a 350 nm cut on filter. The temporal evolution of the LIF signal was recorded by varying the time delay between the photolysis and probe laser. A typical time-revolved LIF profile (Figures 2 and 4) consisted of

between 150 and 250 delay steps, and resulted from the average of between 5 and 10 individual delay scans.

In the experiments monitoring LIF from PO_2, the raw PMT signal needed to be corrected for chemiluminescence produced following the photolysis of $POCl_3$ and PCl_3 in the presence of O_3. Although this chemiluminescence has been observed in other studies involving oxygen-phosphorus systems,[38-41] the precise reactions producing it are unknown, although two studies[38, 41] do suggest it arises from PO_2 itself. Indeed the observed loss of the chemiluminescence signal with [O_3] was consistent with the observed loss of the PO_2 LIF signal with [O_3], suggesting PO_2^* as a possible source. However, of the possible reactions forming PO_2 explored in section 3.2 below, only the reaction between PO and O_3 is sufficiently exothermic to populate the first excited state of PO_2, which lies ~ 250 kJ mol^{-1} above the ground state.[42] As PO may only be produced in experiments using PCl_3 as a precursor (see scheme 3 in section 3.2), this reaction cannot explain the chemiluminescence observed when using $POCl_3$ as a precursor. Furthermore, the observed growth of the chemiluminescence signal with [O_3] was typically only around half the observed growth of the PO_2 LIF signal with [O_3], suggesting a species other than PO_2 as the source of the chemiluminescence. As the exact nature of the chemiluminescence signal is uncertain, its contribution to the raw PMT signal was removed. To do this, back-to-back experiments were conducted, one with the probe laser on, and one with the probe laser off (Figure 4a). In the experiment with the probe laser off, all signal measured by the PMT results from chemiluminescence initiated by the photolysis laser. In the experiment with the probe laser on, the measured signal contained both chemiluminescence initiated by the probe laser, and signal from the LIF of PO_2. The PO_2 LIF signal (Figure 4) is then obtained by subtraction. Note that although chemiluminescence would also have been produced in the experiments monitoring PO LIF signal, no correction to the raw PMT signal was required as the chemiluminescence was effectively excluded by the interference filter used in those experiments.

2.2 PO LIF spectrum

PO LIF spectra were collected using the same experimental setup as the kinetics experiments. PO radicals were generated either by the reaction with O_2 of ground- and excited-state P atoms produced from the multiphoton dissociation of PCl_3 or PBr_3 at 248 nm, or directly from the multiphoton dissociation of $POCl_3$ at 248 nm. These three regimes were used to ensure a positive identification of PO. In the experiments in which LIF spectra were collected, the delay between the photolysis and probe lasers was fixed, while the probe laser wavelength was linearly scanned between 245 and 248 nm. In this manner, each new laser pulse produced the PO LIF signal at a new wavelength, rather than at a later delay time. The pulse width of the probe laser employed is 6 ns, with a linewidth of 0.003 nm. The output of the probe laser was calibrated using a wavemeter (Bristol Wavemeter 871).

Materials

He (99.999 %, BOC), N_2 (99.9995 %, BOC), O_2 (99.999 %, BOC), CO_2 (99.999 %, BOC) were used without further purification. PCl_3 (≥ 99.0 %, VWR), $POCl_3$ (99 %, Sigma Aldrich), dimethyl methylphosphonate (DMMP) (97 %, Sigma Aldrich) were initially degassed by freeze-pump-thawing to remove volatile contaminants, and then made up as dilute vapours in N_2 or He.

3. Results

3.1 PO + O_2

We initially thought that the rate of the reaction between PO and O_2 (R2) could be determined from the PO LIF profiles produced following PLP of PCl_3 in the presence of O_2, via the following reaction scheme:

$$P(^4S) + O_2 \rightarrow PO + O \quad \text{(R1)}$$

$$PO + O_2 \rightarrow PO_2 + O \quad \text{(R2a)}$$

However, as discussed previously,[8] the multiphoton dissociation of PCl_3 produces significant amounts of the first two excited states of P (the ^2D and ^2P states, hereafter collectively referred to as P^*). The formation of P^* together with ground state $P(^4S)$ complicated the reaction scheme so that information regarding the removal of PO could not be extracted. Therefore, in order to measure the rate of reaction R2, a photolytic source of PO was used. Previous studies into the rate of reaction R2 employed DMMP as a PO precursor.[15-17] However, we observed that photolysis of DMMP at 248 nm produced substantial amounts of P*. Indeed, photolysis of DMMP produced so much $P(^2P)$ that we were able to use it as precursor when measuring the rate of $P(^2P)$ with O_2.[8] The formation of P^* from the multiphoton dissociation of DMMP resulted in the reaction scheme for PO formation and removal becoming over complicated, making information regarding the removal of PO difficult to extract. This led us to investigate a cleaner source of photolytic PO. Tests on the PLP of phosphoryl chloride, $POCl_3$, indicated that it was a good source of PO, and did not produce any evidence of P^* formation, even when using concentrations of $POCl_3$ and photolysis energies substantially higher than required for the kinetics experiments. We cannot rule out the significant formation of ground state $P(^4S)$, as we are unable to observe this species directly. However, as the formation of PO from the reaction of $P(^4S)$ and O_2 (R1) would occur on a much longer timescale than the removal of the photolytically produced PO with O_2,[16] this would not affect the measurement of the rate of R2. Numerical simulations of the system (using the chemical kinetics software Kintecus[43]), involving reactions R1 and R2, indicate that 5 times more $P(^4S)$ than PO would need to be produced from the photolysis of $POCl_3$ in order to reduce the measured rate of R2 by only 6 %, a scenario that is unlikely to occur due to the large amount of energy required to produce $P(^4S)$ from $POCl_3$.

A typical PO LIF profile produced following PLP of $POCl_3$ in the presence of O_2 is shown in Figure 2, which demonstrates a small growth of the PO LIF signal at short times.. We attribute this small growth to the formation of rotationally excited PO^* during photolysis, which is then rapidly relaxed to the chamber temperature by the N_2 bath gas. No consideration of vibrational relaxation is required, firstly as vibrational relaxation has been

shown to be much slower than reactive removal of PO (v = 0),[16] and secondly as PO LIF spectra collected when using $POCl_3$ as a precursor indicate no vibrationally excited (v = 1) PO is formed (Figure 6). Thus, the reaction scheme for the formation and removal of PO (v = 0) is given by:

$$POCl_3 + h\nu \rightarrow PO, PO^* + \text{co-products} \quad \text{(R10)}$$

$$PO^* (+ N_2) \xrightarrow{k_{rel}} PO \quad \text{(R11)}$$

$$PO + O_2 \xrightarrow{k_2} \text{loss} \quad \text{(R2)}$$

where PO^* is an initially rotationally excited PO molecule formed from the photolysis of $POCl_3$, k_{rel} is the combined rate coefficient for relaxation of any rotationally excited PO, and k_2 is the bimolecular rate coefficient for the reaction of ground state PO with O_2. As experiments were carried out under pseudo-first order conditions ([PO] « [O_2]), the temporal evolution of the PO is given by:

$$[PO]_t = \left(\frac{k_{rel}}{k' - k_{rel}}\right)[PO^*]_0\left(e^{-k_{rel}.t} - e^{-k'.t}\right) + [PO]_0 e^{-k'.t} \quad \text{(E1)}$$

and

$$k' = k_2[R] + k'_{diff} \quad \text{(E2)}$$

where $[PO]_0$ and $[PO^*]_0$ are the initial concentrations of PO and PO* produced from reaction R10 respectively, t is the time delay between the photolysis and probe lasers, k' is the pseudo-first order rate constant for the removal of PO (i.e., $k_2[O_2]$), and k'_{diff} is the total rate coefficient for other minor loss processes of PO (such as diffusion out of the probe laser beam and reaction with the $POCl_3$ precursor). Equation E1 was fitted to the PO profiles to extract the parameters k_{rel}, k', $[PO]_0$, and $[PO^*]_0$. A plot of k' *vs* [O_2] then yields a straight line of gradient k_2 and intercept k'_{diff}. The inset in Figure 3 shows an example of such a plot, and the small intercept (relative to the total removal rate) demonstrates that reaction with O_2 dominates PO removal. For a given experimental run (in which the temperature and total pressure are kept constant), the parameter k_{rel} was found to be effectively independent of [O_2], over the range employed (typically 0 – 2 × 10^{15} molecule cm^{-3}). This allowed us to do a global fit of the PO traces from an experimental run, with a single fitted value for k_{rel}. For different experimental runs, k_{rel} varied linearly with pressure (see Table 1), as would be expected of rotational relaxation processes. When fitting a biexponential growth and loss, if the growth and loss rates are approaching one another, the fitting procedure is sometimes unable to find a unique solution and returns a result in which the growth and loss rates are equal, meaning one rate has been artificially inflated, and the other decreased. This can be a source of error when analysing biexponential profiles. To minimise the possibility of this affecting our results, for a given pressure (and thus k_{rel}), the [O_2] range was selected to ensure that, even at the highest [O_2], the removal rate was around 4 times lower than the growth rate.

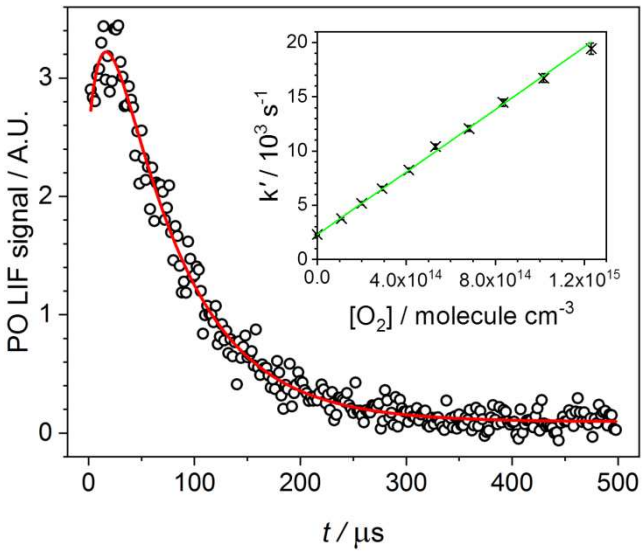

Figure 2. PO LIF signal following PLP of $POCl_3$ at a total pressure of 19.8 Torr and $[O_2]$ = 8.35×10^{14} molecule cm^{-3}, at T = 335 K. Inset: a bimolecular plot for reaction R3 at T = 335 K, giving $k_2 = (1.44 \pm 0.03) \times 10^{-11}$ cm^3 $molecule^{-1}$ s^{-1}.

The bi-molecular rate coefficients for the reaction of PO with O_2 (R2) are presented as a function of temperature in Table 1 and Figure 3a, and compared with available literature. No effects were observed on the bimolecular rate coefficients determined in this study as the radical concentration and photolysis energy were varied by around a factor of 2. The temperature range over which R2 could be studied was limited by thermal decomposition of the $POCl_3$ precursor at temperatures higher than ~ 350 K, which resulted in a large background signal of PO, and a PO removal rate with O_2 that appeared to be ~ 1000 times slower than that measured at ~ 340 K. At the lowest temperature that we investigated (~ 191 K), loss of PO signal indicated significant freezing out of $POCl_3$ on the walls of the reaction chamber. As PO fluorescence is also quenched by the N_2 bath gas, we were unable to go above pressures of ~ 6 Torr at this temperature, due to loss of the PO signal. At temperatures of ~ 294 and 338 K, rate coefficients were measured over the pressure range of ~ 10 – 40 Torr. At both these temperatures, plotting the biexponential rate coefficients *vs* the total bath gas concentration (Figures 3b and 3c), suggests evidence for a small positive pressure dependence, which would be due to a three-body removal channel:

$$PO + O_2 (+ M) \rightarrow PO_3 \qquad \Delta H^\circ_{(0\,K)}\ (kJ\ mol^{-1}) = -416 \qquad (R2b)$$

An Arrhenius fit to the experimental data (dotted line Figure 3a) yields k_2 (PO + O_2, 191 – 339 K) = $(1.91 \pm 0.33) \times 10^{-11} \times \exp^{(-84 \pm 52)/T}$. This fit was determined after increasing the errors at temperatures 294 and 338 K to 10 % of their mean value to avoid the fit being overly weighted to some of the rate coefficients with smaller statistical errors.

In addition to monitoring the loss of PO, experiments were also carried out in which the growth of the PO_2 product from R2 was monitored. These experiments confirmed PO_2 as a product of reaction R2, and the observed rise of PO_2 was consistent with the measured rate

of removal of PO with O_2. However, due to the poor signal to noise of these experiments, no rate coefficients for reaction R2 were determined monitoring the growth of the PO_2 product.

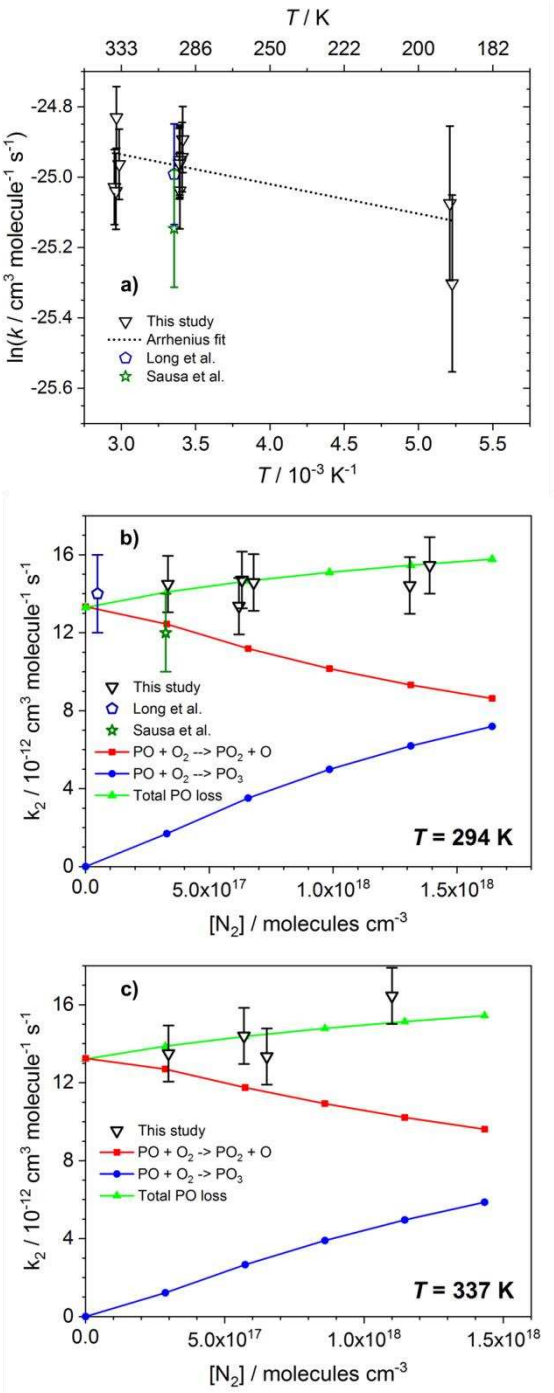

Figure 3. Experimentally determined rate coefficients for the reaction of PO + O_2 vs temperature (a). Pressure dependence of the PO + O_2 reaction at: b) T = 294 K and c) T = 337 K. Open symbol are experimental data from: this study (black downward facing triangles); Long *et al.*[16] (dark blue pentagon); Sausa *et al.*[17] (dark green star). Solid symbols and lines are rates calculated by MESMER[44] for: PO + O_2 → PO_2 + O (channel R2a, red squares); PO + O_2 (+N_2) → PO_3 (channel R2b, blue diamonds); total reaction PO + O_2 (R2, green upward

facing triangles). The dotted line is an Arrhenius fit to the experimental data. At temperatures of 294 and 337 K, experimental errors have been increased to 10 % of their mean value to avoid any one point being overly weighted.

Table 1. Rate coefficients for the reaction of PO + O_2 and relevant experimental conditions (errors are statistical at the 1σ level). *Literature values taken from: [a]Aleksandrov *et al.*[14], full detail of experiment unavailable; [b]Wong *et al.*[15]; [c]Sausa *et al.*[17]; [d]Long *et al.*[16].

Reaction	Precursor	Excitation λ	T (K)	Bath gas	Pressure (Torr)	k_2 (× 10^{-11} cm^3 $molecule^{-1}$ s^{-1})	k'_{diff} (s^{-1})	k_{rel} (× 10^3 s^{-1})
PO + O_2	$POCl_3$	246.3	191	N_2	5.8	1.03 ± 0.26	1279 ± 891	57 ± 11
	$POCl_3$	246.3	192	N_2	6.1	1.29 ± 0.28	791 ± 246	44 ± 3
	$POCl_3$	246.3	295	N_2	10.2	1.45 ± 0.07	1943 ± 103	62 ± 5
	$POCl_3$	246.3	295	N_2	18.9	1.34 ± 0.06	2640 ± 169	89 ± 10
	$POCl_3$	246.3	293	N_2	19.2	1.47 ± 0.09	2692 ± 196	81 ± 2
	$POCl_3$	246.3	295	N_2	20.7	1.46 ± 0.06	2509 ± 122	88 ± 8
	$POCl_3$	246.3	295	N_2	40.2	1.44 ± 0.07	3989 ± 265	183 ± 30
	$POCl_3$	246.3	293	N_2	42.2	1.55 ± 0.10	2161 ± 2285	187 ± 26
*a			300			0.022 ± 0.010		
*b	DMMP	~ 325	303	Ar	~ 2.4	$0.02^{+0.02}_{-0.01}$		
*c	DMMP	246.3	298	O_2	~ 10	1.2 ± 0.2		
*d	DMMP	246.3	298	O_2	~ 1.5	1.4 ± 0.2		
	$POCl_3$	246.3	339	N_2	10.5	1.35 ± 0.05	1935 ± 110	53 ± 4
	$POCl_3$	246.3	335	N_2	19.8	1.44 ± 0.03	2296 ± 91	77 ± 8
	$POCl_3$	246.3	337	N_2	22.8	1.33 ± 0.07	1814 ± 134	99 ± 17
	$POCl_3$	246.3	337	N_2	38.4	1.65 ± 0.10	3224 ±281	132 ± 20

3.2 PO_2 + O_3

A typical PO_2 LIF profile produced following the photolysis of $POCl_3$ in the presence of O_3 can be seen in Figure 4b. Unlike the experiments monitoring PO fluorescence, the 248 nm photolysis laser did not need to be focused in order to observe PO_2, suggesting only a single photon is required to initiate the reaction leading to PO_2. Energetically, a single 248 nm photon has enough energy to remove either 1 Cl atom (R12), or 2 atoms as Cl_2, from $POCl_3$. However, using the time-dependent density functional (TD-DFT) excited states method,[45] within the Gaussian 16 suite of programs,[46] shows that at the TD//B3LYP/6-311+g(2d,p) level of theory, vertical excitation of $POCl_3$ to its first excited state (relevant for a 248 nm photon), and then allowing the molecule to relax, there is clear dissociation to $POCl_2$ + Cl. Thus, we propose the following reaction scheme for the formation of PO_2:

$$POCl_3 + h\nu \rightarrow POCl_2 + Cl \qquad \Delta H^\circ_{(0\,K)}\ (kJ\ mol^{-1}) = +\ 365 \qquad R12$$

$$POCl_2 + O_3 \xrightarrow{k_{13}} PO_2 + Cl_2 + O_2 \qquad \Delta H^\circ_{(0\,K)}\ (kJ\ mol^{-1}) = -\ 127 \qquad R13$$

where k_{13} is the bimolecular rate coefficient for the reaction of $POCl_2$ with O_3. Together with reaction for the removal of PO_2 (R3):

366 $PO_2 + O_3 \xrightarrow{k_3} PO_3 + O_3$ R3

367 and as experiments were carried out under pseudo-first order conditions ([PO_2] « [O_3]), the
368 temporal evolution of PO_2 is given by:

369 $$[PO_2]_t = \left(\frac{k'_{growth}}{k'_{loss}-k'_{growth}}\right)[POCl_2]_0\left(e^{-k'_{growth}\cdot t} - e^{-k'_{loss}\cdot t}\right) \quad \text{(E3)}$$

370 where k'_{growth} and k'_{loss} are the pseudo-first order rate coefficients for the reactions producing
371 and removing PO_2, and $[POCl_2]_0$ is the initial amount of $POCl_2$ formed following photolysis
372 of $POCl_3$. Equation E3 was fitted to the PO_2 profiles (Figure 4b) and the parameters k'_{growth}
373 and k'_{loss}, and $[POCl_2]_0$ extracted. Plots of the parameters k'_{growth} and k'_{loss} should then yielded
374 straight lines, with gradients equal to the bimolecular rate coefficients for reactions R3 and
375 R13 (Equation E2). As we have discussed previously,[8] when analysing biexponential traces
376 some prior knowledge about the system is required to determine whether k'_{growth}, and thus the
377 plot of k'_{growth} vs [O_3], relates to the reaction producing or removing PO_2, and vice versa for
378 k'_{loss} i.e., we need to know which reaction is faster than the other one. As there have been no
379 previous studies of either reaction R3 or R13, this problem was solved by carrying out some
380 additional experiments using PCl_3 as a precursor. This second set of experiments would again
381 yield two bimolecular rate coefficients, one for the production and one for the removal of
382 PO_2. Comparing the two pairs of rate coefficients, one rate coefficient (for the removal of
383 PO_2 by O_3, R3) should be common to both and thus identifiable.

384

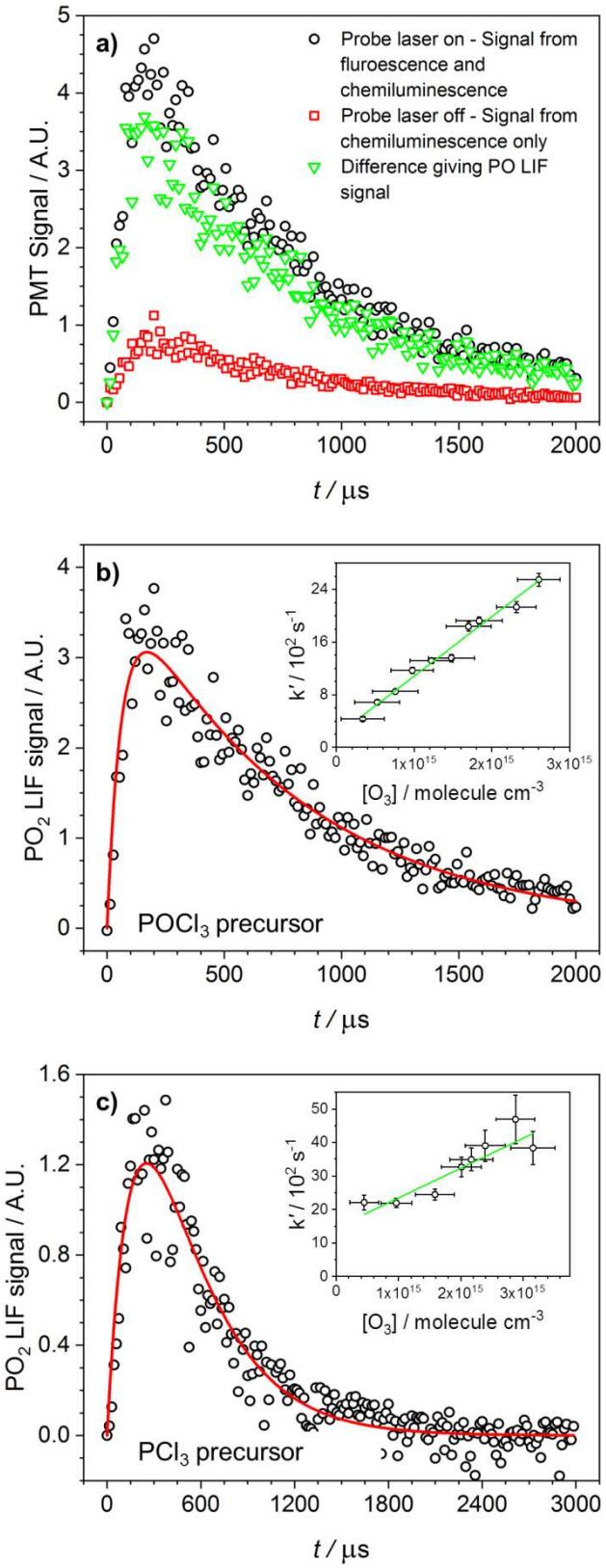

Figure 4. a) PMT signal detected following the photolysis of $POCl_3$ in the presence of O_3, both with (black circles), and without (red squares) the probe laser. The PO_2 LIF signal (green triangles) is then the difference of the two traces. b) PO_2 LIF signal following PLP of $POCl_3$ precursor at a total pressure of 10.6 Torr and $[O_3] = 1.6 \times 10^{15}$ molecule cm^{-3}, at T =

337 K. Inset: bimolecular plot for reaction R3 at T = 337 K, giving k_3 = (9.32 ± 1.37) × 10^{-13} cm^3 $molecule^{-1}$ s^{-1}. c) PO_2 LIF signal following PLP of PCl_3 precursor at a total pressure of 9.36 Torr and [O_3] = 3.8 × 10^{15} molecule cm^{-3}, at T = 292 K. Inset: bimolecular plot for reaction R3 at T = 291 K, giving k_3 = (9.51 ± 2.79) × 10^{-13} cm^3 $molecule^{-1}$ s^{-1}.

A typical PO_2 LIF profile produced following the photolysis of PCl_3 in the presence of O_3 can be seen in Figure 4c. As with the experiments conducted using $POCl_3$ as a precursor, the 248 nm photolysis laser did not need to be focused in order to observe PO_2, suggesting that only a single photon is required to initiate the reaction leading to PO_2. Energetically, a single 248 nm photon has enough energy to remove either 1 Cl atom, or 2 Cl atoms as Cl_2, from PCl_3. The first excited state of PCl_3 is 480 kJ mol^{-1} vertically above the ground state (at the TD//B3LYP/6-311+g(2d,p) level of theory,[9]) which is very close to the energy of a single 248 nm photon. A relaxed scan of the potential surface of this excited state shows that it should dissociate to PCl_2 + Cl. We therefore propose one of the two following reaction schemes for the formation of PO_2 when using PCl_3 as a precursor:

Scheme 1		Scheme 2	
$PCl_3 + h\nu \rightarrow PCl_2 + Cl$	+ 325 kJ mol^{-1}	$PCl_3 + h\nu \rightarrow PCl_2 + Cl$	+ 325 kJ mol^{-1}
$PCl_2 + O_3 \rightarrow PO + Cl_2 + O_2$	- 96 kJ mol^{-1}	$PCl_2 + O_3 \rightarrow POCl + Cl + O_2$	- 216 kJ mol^{-1}
$PO + O_3 \rightarrow PO_2 + O_2$	- 414 kJ mol^{-1}	$POCl + O_3 \rightarrow PO_2 + Cl + O_2$	- 43 kJ mol^{-1}

From our experiments we are unable to tell definitively whether one or the other (or both) of these schemes forms the observed PO_2. Nevertheless, the PO_2 traces can be satisfactorily fit using a biexponential (Figure 4c), where the formation of PO_2 is treated as a single process, described by the term k_{PO_2}. With the substitution of the $[POCl_2]_0$ term with the term $[PCl_2]_0$ (the initial amount of PCl_2 formed following photolysis of PCl_3), we were able to fit the PO_2 traces using equation E3 and extract the parameters, k'_{growth}, k'_{loss}, and $[PCl_2]_0$. Plots of k'_{growth} and k'_{loss} *vs* [O_3] then yielded straight lines with gradients equal to the bimolecular rate coefficients k_{PO_2} and k_3, and intercepts k'_{diff} (equation E2).

Figure 5 shows the rate coefficients obtained when using both $POCl_3$ and PCl_3 as a precursor. At T ~ 293 K the rate coefficients obtained by plotting k'_{growth} *vs* [O_3] for the different precursors differ significantly (Figure 5a), ranging from (7.11 ± 0.74) × 10^{-12} cm^3 $molecule^{-1}$ s^{-1} for $POCl_3$ to only (1.54 ± 0.37) × 10^{-12} cm^3 $molecule^{-1}$ s^{-1} for PCl_3. In contrast, there is quite good agreement between the rate coefficients obtained by plotting k'_{loss} *vs* [O_3] for the different precursors (Figure 5b): (8.93 ± 0.19) × 10^{-13} cm^3 $molecule^{-1}$ s^{-1} for $POCl_3$ *vs* (7.58 ± 0.50) × 10^{-13} cm^3 $molecule^{-1}$ s^{-1} for PCl_3. This implies that k'_{growth} describes the reactions forming PO_2, while k'_{loss} describes the reaction removing PO_2, R3. With this assignment, k_3 was determined over a range of temperatures and pressures (Figure 5 and Table 2). k_3 did not vary significantly as radical concentrations and photolysis energies were varied by a factor of ~2, or pressures varied by a factor of ~6. The upper temperature limit at

which k_3 could be studied was set by the thermal decomposition of O_3 on the reactor walls at temperatures higher than 380 K. An Arrhenius fit (dotted line in Figure 5b) to the experimental data yields $k_3(PO_2 + O_3, 186 - 339\ K) = (2.2 \pm 0.7) \times 10^{-11} \exp^{(-990 \pm 81)/T}$ cm^3 molecule^{-1} s^{-1}.

A possible source of error in the determination of k_3 is interference from O atoms produced from the photolysis of O_3. These O atoms may react with either the precursors or other photolysis products to form PO_2. As discussed above, between 10 and 20 % of the O_3 at the interaction region is photolysed by the 248 nm photolysis laser. Photolysis of O_3 at 248 nm produces either excited state $O(^1D) + O_2$ with a quantum yield of 0.9, or ground state $O(^3P) + O_2$ with a quantum yield of 0.1.[37] The excited $O(^1D)$ atoms will be rapidly relaxed down to ground state $O(^3P)$ by collisions with the N_2 bath gas. This relaxation occurs on a significantly faster timescale than the observed growth of PO_2 when using either precursor (~ 200 times faster at a pressure of 5 Torr), suggesting that reaction of $O(^1D)$, either with the precursors or other photolysis products, is not a significant source of PO_2. With regards to reaction of the relaxed $O(^3P)$ with the precursors, with $POCl_3$ the reaction to $PO_2 + Cl_2 + Cl$ is thermodynamically unfavourable, being endothermic by ~ 120 kJ mol^{-1}. In contrast, for the reaction of $O(^3P)$ with $POCl_2$ there are two energetically viable reactions:

$$POCl_2 + O(^3P) \rightarrow PO_2 + Cl_2 \qquad \Delta H^\circ_{(0\ K)}\ (\text{kJ mol}^{-1}) = -226 \qquad \text{R14a}$$

$$POCl_2 + O(^3P) \rightarrow PO_2Cl + Cl \qquad \Delta H^\circ_{(0\ K)}\ (\text{kJ mol}^{-1}) = -317 \qquad \text{R14b}$$

The more exothermic channel (R14b), which also involves a single bond cleavage, should be favoured, suggesting the contribution of reaction R14a to the PO_2 observed in our experiments is likely to minor. However, as we are not able to unequivocally rule out contribution from reaction R14a, numerical simulations using Kintecus[43] have been conducted, in which for a range of experimentally applicable $[O_3]$ and [O], the rates of R13 and R14a were varied and their effect on the determined rate of R3 evaluated. In these simulations, k_{13} was varied between 0 and 8×10^{-12} cm^3 molecule^{-1} s^{-1}, while k_{14a} was varied from 0 up to 1×10^{-10} cm^3 molecule^{-1} s^{-1} (using values higher than these upper limits results in the gradient of a plot of k'_{growth} *vs* $[O_3]$ being larger than that observed experimentally). The numerical simulations showed that the rate coefficient determined for R3 was unaffected by varying either k_{13} or k_{14a} between the ranges given. Thus, the occurrence of the side reaction R14a producing PO_2 in our experiments would not have affected the value determined for k_3. The reason for this is due to the approximately linear relationship between $[O_3]$ and [O] in our experiments (at high $[O_3]$ the percentage of O_3 photolysis at the interaction region is smaller than at low $[O_3]$, so the relationship is not precisely linear). Whether PO_2 is produced from the reaction of $POCl_2$ with O_3 (R13) or from the reaction of $POCl_2$ with $O(^3P)$ (R14a), or from a combination of both, as a doubling of the concentration of O_3 will be mirrored by an approximately doubling of the concentration of $O(^3P)$, the rate of PO_2 formation will also be doubled. As such, we are able to fit a biexponential (rather than a tri- or higher exponential) to our PO_2 LIF traces to extract the pseudo-first order rate coefficients, and the value determined for k_3 is unaffected.

With regards to the reaction of $O(^3P)$ with the PCl_3 precursor, there are energetically viable pathways to $POCl_2$ and POCl, both of which could go on to react with O_3 or another

$O(^3P)$ to produce PO_2. However, there are two reasons we can rule out $O(^3P)$ reacting with the PCl_3 precursor as a source of PO_2. First, if this were the case, as PCl_3, $O(^3P)$, and O_3 are all in excess in our experiments, we would expect to see vastly more PO_2 LIF signal in experiments using PCl_3 as a precursor than in experiments using $POCl_3$, in which PO_2 is only produced from reaction of the deficient $POCl_2$ photolysis product. Second, if a reaction between $O(^3P)$ and PCl_3 was generating PO_2, we would expect the PO_2 LIF signal to be directly proportional to $[O(^3P)]$ (and thus $[O_3]$). As neither of these cases are true, the reaction between $O(^3P)$ and PCl_3 can be ruled out as a source of PO_2. For the reaction of $O(^3P)$ with PCl_2, there are energetically viable product channels, producing either PO or POCl. This leads us to suggest a further two reaction schemes for the formation of PO_2 when using PCl_3 as a precursor:

Scheme 3		Scheme 4	
$PCl_3 + h\nu \rightarrow PCl_2 + Cl$	+ 325 kJ mol^{-1}	$PCl_3 + h\nu \rightarrow PCl_2 + Cl$	+ 325 kJ mol^{-1}
$PCl_2 + O(^3P) \rightarrow PO + Cl$	- 195 kJ mol^{-1}	$PCl_2 + O(^3P) \rightarrow POCl + Cl$	- 315 kJ mol^{-1}
$PO + O_3 \rightarrow PO_2 + O_2$	- 414 kJ mol^{-1}	$POCl + O(^3P) \rightarrow PO_2 + Cl$	- 142 kJ mol^{-1}

From our experiments we are unable to tell which of the four reaction schemes involving PCl_2 reacting with O_3 or $O(^3P)$, or combination thereof, are generating PO_2 in our experiments. Nevertheless, as stated above, the PO_2 traces were satisfactorily fit using the biexponential given in Equation E3 (Figure 4c). Furthermore, the numerical simulations on the $POCl_2$ with O_3 and $O(^3P)$ system indicated that whether PO_2 is generated from reactions of O_3 or $O(^3P)$, the rate coefficient determined for R3 was unaffected due to the approximately linear relationship between $[O_3]$ and $[O(^3P)]$. As such, we expect any contribution from schemes 3 and 4 to the production of PO_2 to have little effect on k_3.

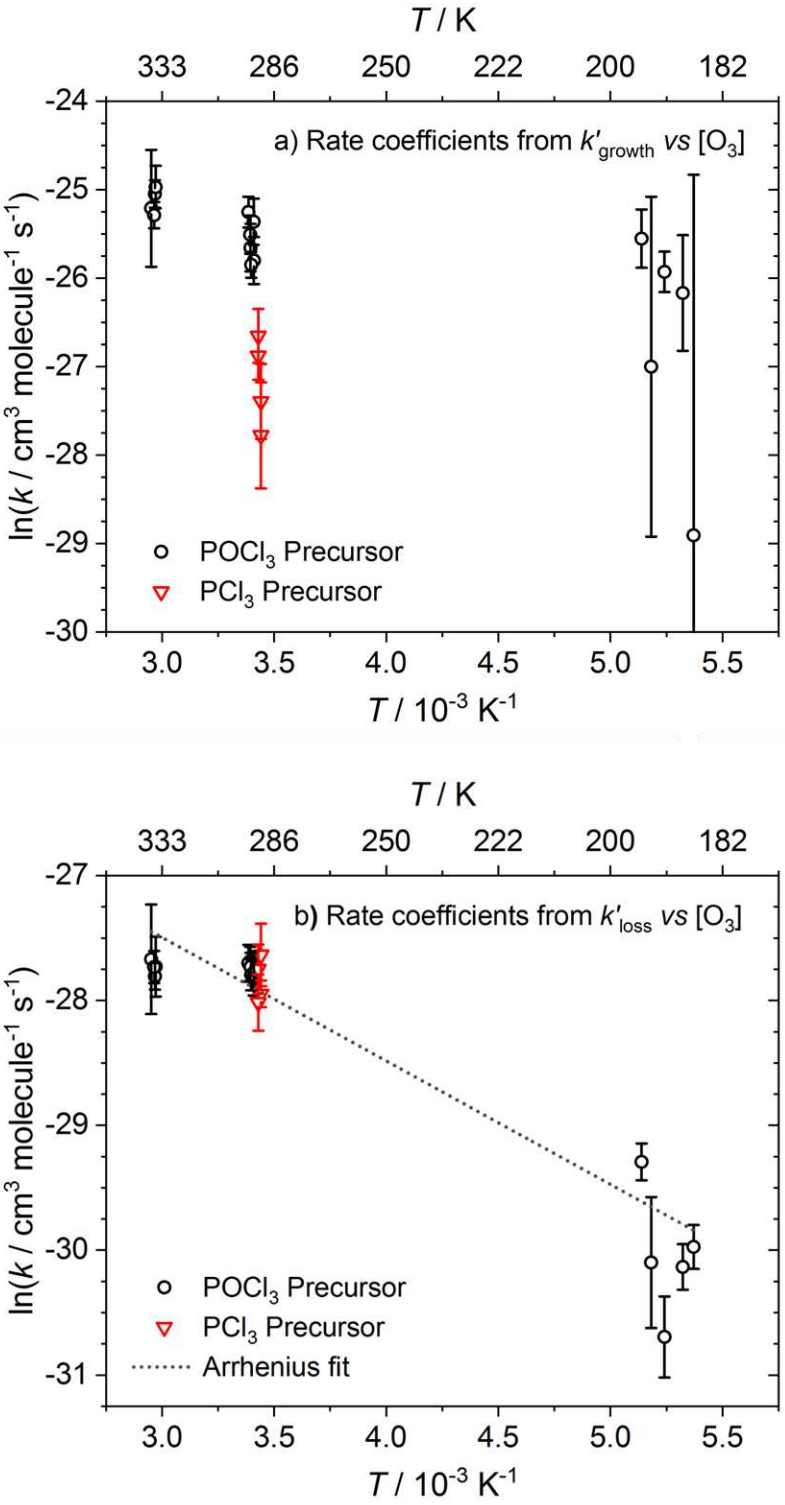

Figure 5. Bimolecular rate coefficients determined by plotting: a) k'_{growth} *vs* [O_3] and determined to relate to reactions R13 and/or R14b (for $POCl_3$ as a precursor), and the summed processes forming PO_2 (for PCl_3 as a precursor); and b) k'_{loss} *vs* [O_3] and determined to relate to reaction R3. Black circles are experiments using $POCl_3$ as a precursor, while red triangles are those using PCl_3 as a precursor. The dotted line is an Arrhenius fit.

Table 2. Rate coefficients for reaction of $PO_2 + O_3$ and relevant experimental conditions (uncertainties reported at the 1 σ level for the linear least-squares fitting of the pseudo first-order coefficients as a function of $[O_3]$)

Reaction	Precursor	Excitation λ	T (K)	Pressure (Torr)	k_3 ($\times 10^{-13}$ cm^3 $molecule^{-1}$ s^{-1})
$PO_2 + O_3$	$POCl_3$	286.1	188	4.49	0.82 ± 0.15
	$POCl_3$	286.1	191	5.48	0.47 ± 0.15
	$POCl_3$	286.1	186	8.22	0.96 ± 0.17
	$POCl_3$	286.1	195	10.48	1.90 ± 0.28
	$POCl_3$	286.1	193	19.91	0.85 ± 0.44
	$POCl_3$	287.0	295	5.26	9.32 ± 1.37
	$POCl_3$	286.1	294	10.18	8.50 ± 1.05
	$POCl_3$	286.1	295	13.1	9.05 ± 1.01
	$POCl_3$	287.0	293	30.0	8.26 ± 1.14
	$POCl_3$	286.1	293	30.2	9.10 ± 1.10
	$POCl_3$	287.0	295	32.4	9.48 ± 1.09
	PCl_3	287.0	291	6.69	6.07 ± 1.85
	PCl_3	287.0	292	9.39	9.85 ± 3.86
	PCl_3	287.0	291	10.37	9.51 ± 2.79
	PCl_3	287.0	292	15.5	6.73 ± 7.57
	$POCl_3$	286.1	337	5.14	9.07 ± 2.17
	$POCl_3$	287.0	339	9.45	9.62 ± 4.22
	$POCl_3$	286.1	337	10.6	9.04 ± 1.16
	$POCl_3$	287.0	337	16.27	8.39 ± 8.95

3.2 PO LIF Spectra

LIF spectra of PO, collected using different PO production regimes, are shown in Figure 6. The good agreement between spectra producing using different precursors allows for a positive identification of PO, while comparison of line positions to earlier emission and fluorescence studies allows for positive identification of the *A-X* system.[17, 28-29, 47] The spectra have been baseline corrected to remove any contribution from scattered probe laser light. No corrections were made to account for laser dye efficiency, or the spectral efficiency of the PMT, as neither of these change significantly over the narrow spectral range of the measurements.

Figure 6 illustrates that there is a significant population of vibrationally excited PO (v = 1) when using PCl_3 or PBr_3 as a precursor, indicating that the reaction of P* + O_2 (and possibly $P(^4S) + O_2$) produces both ground and vibrationally excited PO (v = 1). As with the detection of PO (v = 0), PO (v = 1) is also detected by non-resonant fluorescence *via* the (v',v'' 1,2) transition at ~ 253.6 nm. This is due to the resonant fluorescence being excluded by our interference filter. When using $POCl_3$ as a precursor, we see no evidence of vibrationally excited PO, even at very short delay times (30 μs), indicating that the small growth in PO signal observed in the kinetic traces of PO (Figure 2) is due to rotational relaxation, rather than relaxation of higher vibrational states.

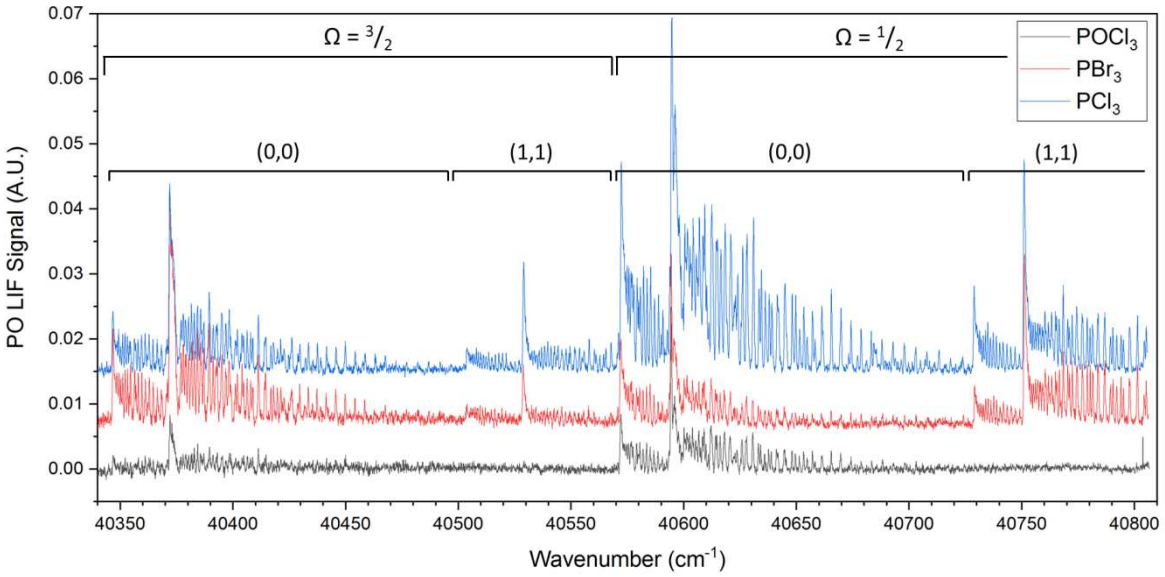

Figure 6. PO LIF spectra taken using three different precursors, together with labels indicating the $X\,^2\Pi_{3/2}$ and $X\,^2\Pi_{1/2}$ sub-bands, and the upper and lower vibrational levels: Blue upper trace – PCl_3; red middle trace – PBr_3; grey lower trace – $POCl_3$.

4. Discussion

4.1 Comparison with previous work

The bimolecular rate coefficients for the removal of PO with O_2 (R2) determined in this study are compared with the literature values in Table 1 and Figure 3. As discussed above, there is significant discrepancy in the literature over the room temperature rate of reaction R2, with two studies reporting a rate constant of ~ 2×10^{-13} cm^3 molecule^{-1} s^{-1},[14-15] and two others a rate constant 60 times faster, of ~ 1.3×10^{-11} cm^3 molecule^{-1} s^{-1}.[16-17] Taking an average of our room temperature measurements, we determine a value of k_2 = (1.44 ± 0.11) × 10^{-11} cm^3 molecule^{-1} s^{-1} at T = 294 K, putting the rate towards the top end of the available literature, in good agreement with the value reported by Long *et al.*[16] and lying slightly above (just outside mutual error limits) the value reported by Sausa *et al.*[17]. The probable reason for the large discrepancy between the measured values of k_2 is the different experimental techniques employed. The two lower values were measured in fast flow tubes, using a microwave discharge of DMMP to produce PO, the loss of which was then monitored using LIF. The two larger rate coefficients were measured by the PLP-LIF technique, similar to that employed in this study, with the exception that DMMP rather than $POCl_3$ was used as the PO precursor. As in the present work, Sausa *et al.*[17] used a KrF excimer laser (248 nm) as the photolysis source. They discuss in their paper that the focused KrF radiation may result in the dissociation of O_2, so that they observed the reaction of PO with O rather than PO + O_2. Indeed they do note a significant deviation from exponential decay of PO when the photolysis source is a shorter wavelength ArF laser (193 nm), which would have generated a much larger fraction of O atoms. However, interference from O atoms can in fact be ruled out,

because Long *et al.*[16] produced PO from the infrared multiphoton dissociation of DMMP, a method which cannot generate O atoms from O_2, and they obtained a value for k_2 in good agreement with that obtained with the KrF lasers employed in the present study and that by Sausa *et al.*[17].

Another possible source of error in measurements of k_2 is interference from P atoms, which has not been discussed in the previous studies. As we have demonstrated previously,[8] multiphoton dissociation of DMMP by focused 248 nm light produces significant amounts of P*. Although not directly detectable in our experiments, we also presume the presence of ground state P(^{4}S), formed either directly from the multiphoton dissociation of DMMP, or from the relaxation of P*. These excited state P* atoms react with O_2 to form PO on a timescale similar to that at which PO is removed by O_2.[8] Thus, if significant amounts of these excited states are present, the observed removal of PO would be slower, resulting in a smaller rate coefficient for the reaction. This may be less of a problem in the study by Long *et al.*[16] in which the photolysis source is 10.6 μm light from an infrared CO_2 laser. At this wavelength, many more photons would need to be absorbed to excite PO to a high enough level in which it may dissociate to ground or excited state P atoms. Indeed, the rate constant measured by Long *et al.*[16] agrees well with that determined in our study where we used a PO precursor that does not produce P* when photolysed. P(^{4}S) atoms also react with O_2 to produce PO (R1), however the timescale of this reaction is around 50 times slower than the removal of PO by O_2, and as such the formation of any ground state P atoms should only have a minor effect on the measurement of k_2 (see Section 3.1).

Figure 3 indicates that there is a small pressure dependence for reaction R2, which is evidence for both a two- and three-body channel for this reaction (R2a and R2b, respectively), which are explored using theoretical calculations in Section 4.2. The presence of the three-body channel forming PO_3 has not previously reported in the literature, presumably as the previous studies did not measure the removal of PO_2 over a range of pressures.

The have been no previous investigation into the kinetics of the reaction between PO_2 and O_3. Taking the average of our room temperature measurements, we determine that $k_3 = (8.47 \pm 0.30) \times 10^{-13}$ cm^3 molecule^{-1} s^{-1} at $T = 293$ K. This is over 4 orders of magnitude faster than the reaction between the isovalent NO_2 with O_3 (~ 3.5×10^{-17} cm^3 molecule^{-1} s^{-1} at $T = 298$ K).[48] Although this reaction is unlikely be important astrochemically, the fact that many current chemical models are using the isovalence between nitrogen and phosphorus to derive rate coefficients for P-bearing species is called into question, and highlights the importance of experimentally determined rate coefficients.

4.2 Theoretical Calculations

Electronic structure calculations were carried out using the Gaussian 16 suite of the programs.[9] Vibrational frequencies, rotational constants and energies were calculated with the Complete Basis Set (CBS-QB3) method of Montgomery et al.[49] The Cartesian coordinates, molecular parameters and heats of formation of the phosphorus oxides are listed in Table 3.

588

589 **Table 3.** Molecular properties of the stationary points on the potential energy surfaces for PO
590 + O_2 and PO_2 + O_3. The molecular geometries are illustrated in Figure 7.

Molecule	Geometry (Cartesian co-ordinates in Å) [a]	Rotational constants (GHz) [a]	Vibrational frequencies (cm^{-1}) [a]	$\Delta_f H^e$ (0 K) (kJ mol^{-1}) [b]
PO + O_2 surface (Figure 7a)				
PO	P, -0.319, 0.057, 0. O, 0.176, -1.341, 0.	21.78779	1247	-31
cis-OPO_2	P, 0.760, 0.487, 0.000 O, 1.208, -0.902, 0.000 O, -0.977, 0.570, 0.000 O, -1.654, -0.583, 0.000	16.31182 5.04050 3.85062	164, 217, 500, 540, 1071, 1300	-150
TS1 (from *cis*-OPO_2 to *trans*-OPO_2	P, 0.896, 0.377, -0.134 O, 1.582, 1.646, 0.097 O, -0.756, 0.712, 0.037 O, -1.976, 0.225, 0.003	35.26271 3.53849 3.21579	209*i*, 94, 342, 547, 1139, 1292	-139
trans-OPO_2	P, -0.549, -0.457, 0.005 O, -1.730, 0.403, -0.001 O, 0.830, 0.613, 0.001 O, 1.934, -0.149, -0.001	32.75631 3.94718 3.52270	105, 246, 370, 638, 1105, 1300	-161
TS2 (from *trans*-OPO_2 to PO_3)	P, -0.332, -0.114, 0.460 O, -1.536, -0.050, 0.389 O, 1.002, 0.809, -0.052 O, 1.161, -0.605, 0.366	18.38211 5.63914 5.25830	1506*i*, 237, 354, 479, 930, 1175	-115
TS3 (from *cis*-OPO_2 to PO_2 + O	P, -0.136, 0.898, -0.071 O, 0.163, 0.149, 1.155 O, -0.244, 0.372, -1.488 O, -0.036, -1.398, -2.161	17.01510 3.67813 3.02436	391*i*, 103, 223, 405, 889, 1264	-29
PO_3	P, 0.000, 0.000, 0.002 O, 0.000, 0.000, 1.479 O, 1.278, 0.000, -0.742 O, -1.278, 0.000, -0.742	9.64387 9.64387 4.82194	192, 192, 434, 1015, 1123, 1123	-447
PO_2 (or OPO)	P, 0.001, 0., 0.000 O, 0.0006, 0., 1.474 O, 1.056, 0., -1.028	98.10129 8.57057 7.88196	388, 1068, 1314	-290
PO_2 (or OPO) [c]	P, 0., 0., 0.276 O, 0., 1.376, -0.269 O, 0., -1.376, -0.269	108.11428 8.33894 7.74181	398, 1077, 1478	-260 [d]
PO_2 + O_3 surface (Figure 7b)				
TS1 (from PO_2 + O_3)	O, 2.091, 0.500, 0.770 O, 2.073, -0.246, -0.284 O, 1.174, -1.168, -0.259 P, -1.332, 0.070, -0.277 O, -2.321, -0.589, 0.605 O, -0.703, 1.407, -0.375 [c]	5.87904 1.52137 1.35133 [c]	36*i*, 38, 63, 66, 99, 176, 400, 699, 1035, 1077, 1101, 1454	-135 [d]
OPO-O_3	P, 0.622, 0.000, 0.000 O, 1.170, -1.344, 0.000 O, 1.169, 1.344, -0.001 O, -1.721, 0.000, 0.000 O, -0.886, 0.000, 1.071 O, -0.887, 0.000, -1.070	5.35021 3.06448 2.71613	201, 215, 227, 346, 374, 411, 447, 819, 924, 1036, 1161, 1458	-380
TS2 (from OPO-O_3 to PO_3 + O_3)	P, -0.676, 0.000, 0.022 O, -1.179, 1.348, -0.166 O, -1.179, -1.348, -0.165 O, 1.749, 0.000, 0.165	5.28567 2.86956 2.56924	144*i*, 123, 234, 314, 383, 403, 552, 734, 828, 1155, 1180,	-370

	O, 0.666, 0.000, 1.113 O, 1.223, 0.000, -1.013		1476	

[a] Calculated at the CBS-QB3 level of theory. [b] Heat of formation at 0 K, using reference values for $P_{(g)}$, O and O_3 of $\Delta_f H^e$ (0 K) = 315.7, 246.8 and 144.5 kJ mol^{-1}, respectively.[50] [c] Calculated at the MP2/6-311+g(2d,p) level of theory. [d]Energy at the CCSD(T)//MP2/6-311+g(2d,p) level of theory.

The resulting potential energy surfaces for PO + O_2 (R2) and PO_2 + O_3 (R3) are shown in Figures 7a and 7b, respectively, which also illustrate the geometries of the stationary points. RRKM calculations were then performed for these two reactions using the Master Equation Solver for Multi-Energy well Reactions (MESMER) program.[44] R2 initially involves addition of O_2 to PO, forming the *cis*-OPO_2 complex. This can either dissociate directly to PO_2 + O *via* TS3, or first rearrange to *trans*-OPO_2 *via* TS1 followed by rearrangement to PO_3 *via* TS2. PO_3 will then either be quenched by collision with the third body (N_2), or dissociate to PO_2 + O.

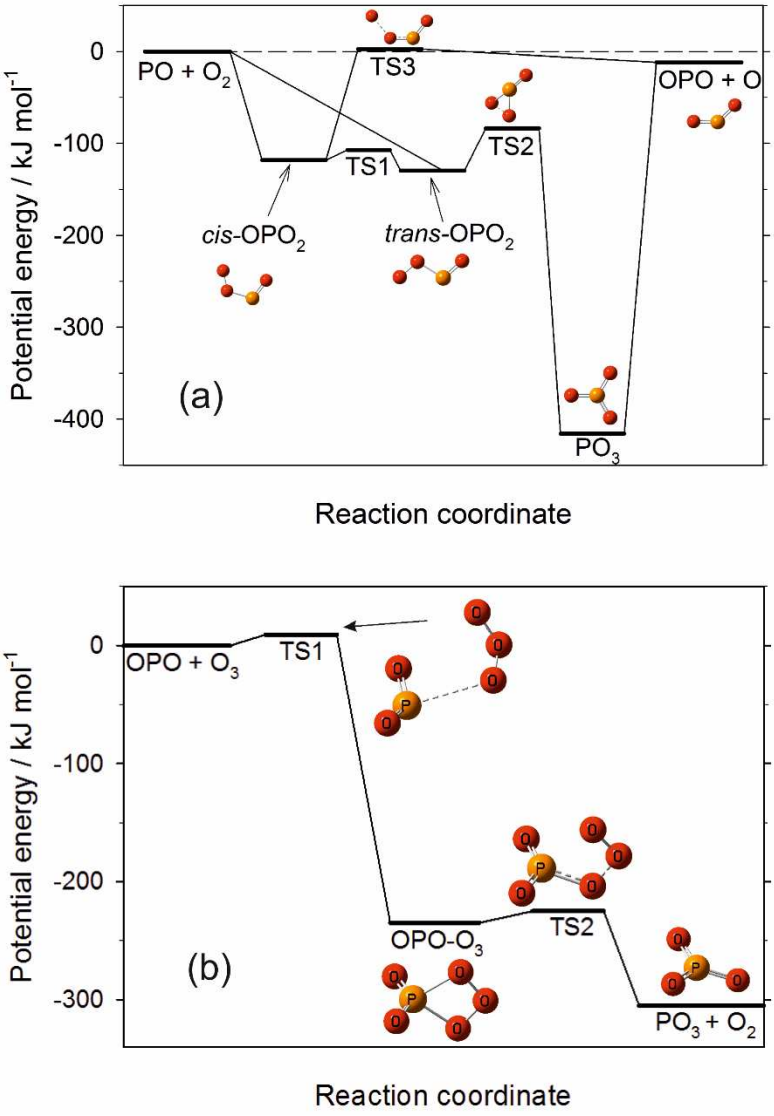

Figure 7. Potential energy surfaces for (a) PO + O_2 (R2), determined at the CBS-QB3 level of theory, and (b) PO_2 + O_3 (R3), determined at the CBS-QB3 level of theory apart from barrier TS1 which is a CCSD(T)//MP2/6-311+g(2d,p) calculation with respect to the reactants.

The internal energy of each species on the potential energy surface was divided into a contiguous set of grains (width 200 cm^{-1}), each containing a bundle of rovibrational states. Each grain was then assigned a set of microcanonical rate coefficients for dissociation back to the reactants (PO + O_2), and forward to the products (PO_2 + O), using an inverse Laplace transformation to link them directly to the high-pressure limiting recombination coefficients (k_∞). An Arrhenius expression was optimised by floating both the pre-exponential factor and the activation energy to give the best fit of the RRKM model to the experimental data, yielding $k_\infty(PO + O_2) = 3.5 \times 10^{-11} \exp^{(-168/T)}$ cm^3 $molecule^{-1}$ s^{-1}. For the reaction of PO_2 + O, the rate coefficient was set to be reasonably fast with a small T-dependence, $k_\infty(PO_2 + O)$ =

619 $2.4 \times 10^{-11} \exp^{(-25/T)}$ cm^3 $molecule^{-1}$ s^{-1}. The exponential down model was used to estimate the
620 probability of collisional transfer between grains. For N_2 as the third body, the average
621 energy for downward transitions $\langle \Delta E \rangle_{down}$ was set to 300 cm^{-1} at 300 K, with a temperature
622 dependence of $T^{0.25}$.[51]

623 Figure 3 shows a satisfactory fit to the experimental data at 294 and 337 K. Figure 8
624 illustrates the RRKM-predicted overall rate coefficient k_2 (Figure 8a) and the branching ratio
625 to produce PO_3, as a function of $[N_2]$ and T (Figure 8b). Figure 8 shows that the variation of
626 the total rate coefficient and the branching ratio to form the two products OPO and PO_3 have
627 relatively complex dependences on P and T. This arises from the nature of the PES for the
628 reaction (Figure 7a). As a result, a Troe-type fall-off expression[52] does not give a good fit to
629 the rate coefficient for the recombination reaction forming PO_3. Nevertheless, the data plotted
630 in Figure 8 can be used to estimate the rate coefficients for both reaction channels at a
631 selected P and T. As shown in Figure 8a, k_2 is predicted to have a rather small T and P
632 dependence. At $[N_2] < 10^{17}$ cm^{-3}, over the temperature range 120 – 500 K, the fraction of PO_3
633 formed is below 1%. At pressures typical of planetary upper atmospheres where meteoric
634 ablation of P will occur,[7] the reaction should essentially be pressure-independent and can be
635 fitted to the following expression: $\log_{10}(k_2,\ 120 - 500\ K,\ cm^3\ molecule^{-1}\ s^{-1}) = -13.915 +$
636 $2.470\log_{10}(T) - 0.5020(\log_{10}(T))^2$, with an uncertainty of ± 10 % within the experimental
637 temperature range (191 – 339 K).

638

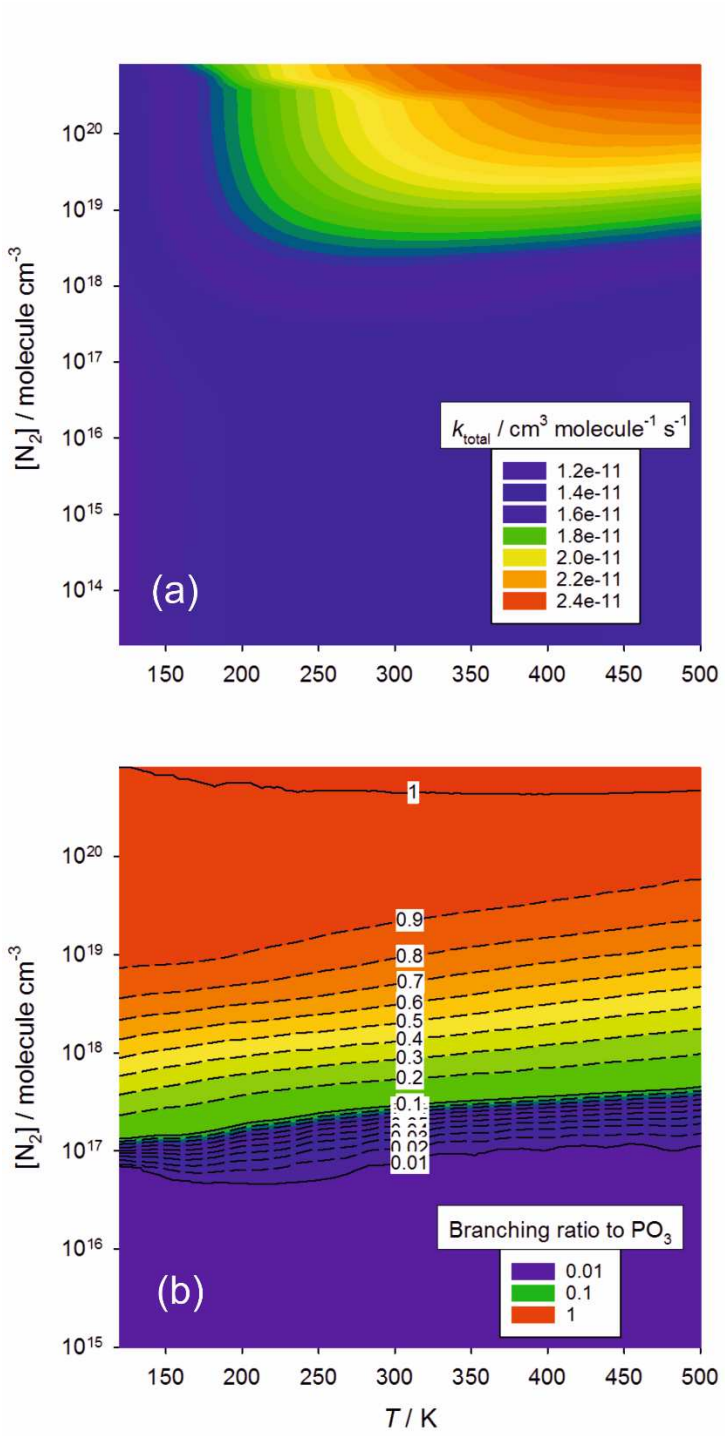

Figure 8. RRKM calculations for the reaction PO + O_2 on the surface in Figure 7a: a) the overall rate coefficient, k_2; b) the branching ratio to PO_3; both plotted as a function of [N_2] and T.

For the reaction between PO_2 and O_3, the RRKM fit using the potential energy surface in Figure 7b was used. The measured positive temperature dependence of the reaction (Figure 5) implies that there is a barrier in the entrance channel. Initial exploration of the reaction entrance channel using the B3LYP/6-311+g(2d,p) level of theory did not indicate the

presence of a barrier. However, this DFT functional is not appropriate for long-range interactions; guided by previous work on the analogous reaction between NO_2 and O_3 (which has a significantly larger barrier in the entrance channel),[53] we used the MP2 level of theory to determine that a small barrier exists at a $PO_2 - O_3$ separation of 2.7 Å. An accurate coupled cluster calculation at the CCSD(T)//MP2/6-311+g(2d,p) level of theory[54] gave a barrier height of 9.4 kJ mol^{-1} (Figure 7b and Table 3), in good agreement with the 8.2 ± 0.7 kJ mol^{-1} activation energy determined from the Arrhenius fit to the experimental data. A satisfactory fit to the experimental data was then obtained by optimising the pre-exponential factor in an Arrhenius expression for the inverse Laplace transformation, yielding $k_\infty(PO_2 + O_3, 180 - 370\ K) = 3.7 \times 10^{-11} \exp^{(-1131/T)}$ cm^3 molecule^{-1} s^{-1} (σ = ± 26 % over the experimental temperature range, 188 – 339 K), where the activation energy is set to 9.4 kJ mol^{-1}.

4.3 Fitting the PO spectra

To simulate the PO spectra obtained in this study, we have used the PGOPHER spectral simulator,[55] together with the molecular constants provided by Verma and Singhal[47] for the $X\ ^2\Pi$ state and by Coquart *et al.*[28] for the $A^2\Sigma^+$ state. The simulated PO spectrum was then compared to the experimental spectrum obtained using PCl_3 as a precursor, which was chosen as it has the best signal-to-noise (although it should be noted that for the lines that are visible in the spectra produced using PBr_3 and $POCl_3$ as precursors, there is excellent agreement between the line positions – Figure 6). Next, the simulated spectrum was refined by first assigning simulated lines to the corresponding peaks in the experimental spectra, then refitting the simulated spectrum to the experimental allowing the molecular constants to float. This process was iterative, with more peaks being able to be assigned and fitted as agreement between the simulated and experimental spectra improved. Both the (0,0) and (1,1) bands were fit simultaneously.

When fitting the spectra, we encountered some difficulty in obtaining a good fit to sections of the fine structure within the (0,0) bands. Verma and Singhal[47] reported that the $A^2\Sigma^+$ (v = 0) level of PO is perturbed by the $^4\Sigma^-$ (v= 4) level. By including this perturbing state in our simulation, we were able to obtain good a fit to the data. Figure 9 shows the simulated spectrum overlaid on the experimental spectrum, as well as the residual for the contour fit, while Tables 4 – 6 give the molecular constants employed in the simulation. The best match was obtained using a rotational temperature of 350 K, and by convolving the simulated spectra with a Gaussian with 0.6 cm^{-1} FWHM, which accounts for Doppler broadening and spectral resolution. In addition to allowing the molecular constants to float, the relative intensities of the $A^2\Sigma^+$ (v = 0) ← $X\ ^2\Pi$ (v = 0), the $A^2\Sigma^+$ (v = 1) ← $X\ ^2\Pi$ (v = 1) transitions were also floated. The $^4\Sigma^-$ (v= 4) ← $A^2\Sigma^+$ (v = 0) matrix element was 4.593 ± 0.011.

As can be seen from Figure 9, there is good agreement between the line positions of the simulated and experimental spectra, for both the (0,0) and (1,1) bands. In general there is also satisfactory agreement between the simulated and experimental line intensities. There does, however seem to be some systematic differences between branches, implying some additional Ω (but not J) dependent mixing between branches. Comparing the molecular

constants obtained in this study with the literature values (Tables 4 – 6) shows that all the values are essentially consistent, with the differences most likely arising from minor differences in the definitions of the constants.

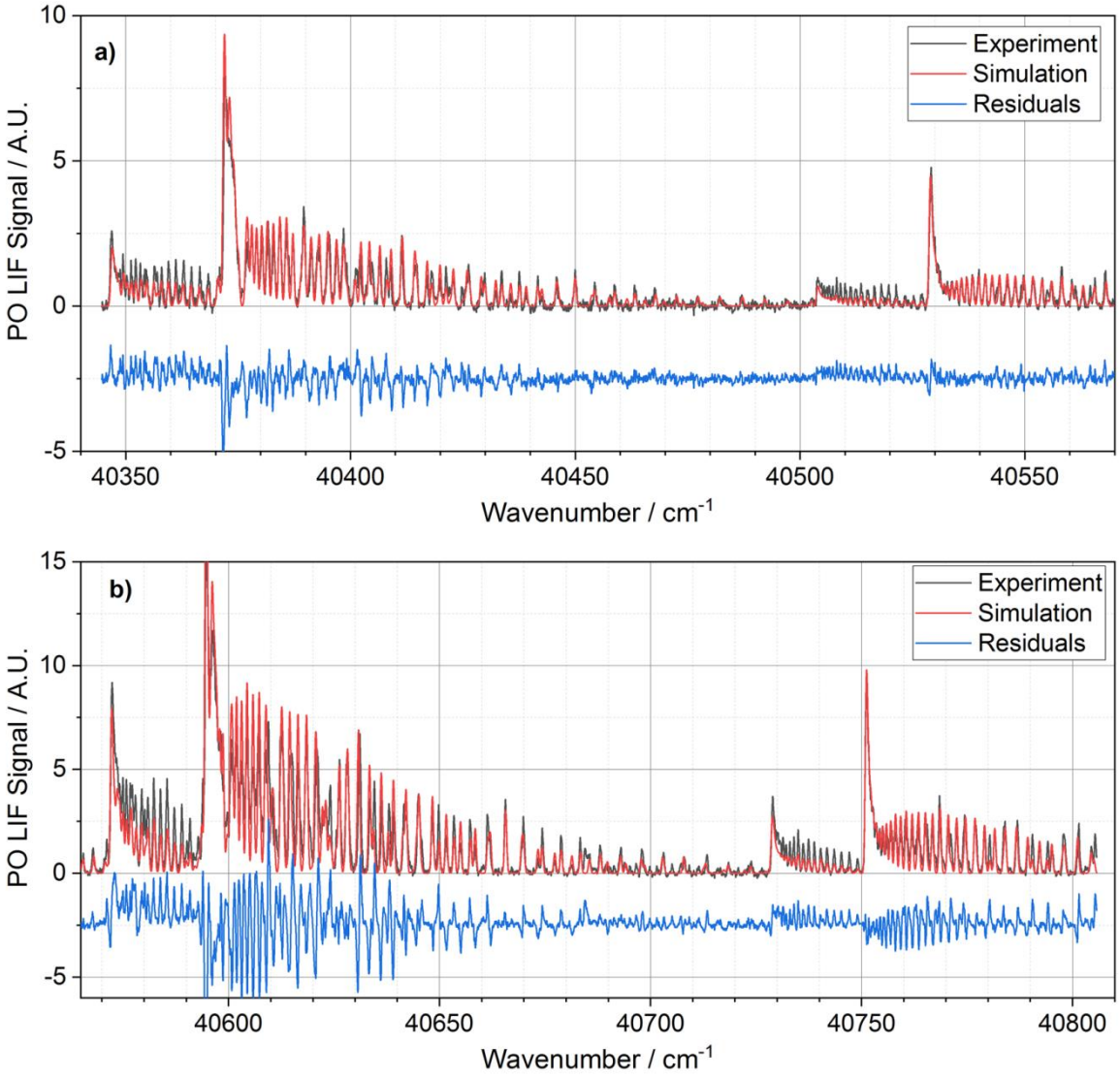

Figure 9: Measured and calculated $A^2\Sigma^+ \leftarrow X\,^2\Pi$ band of PO, together with the residual (experimental – simulated). Plot a) shows the $X\,^2\Pi_{3/2}$ sub-band, while plot b) shows the $X\,^2\Pi_{1/2}$ sub-band.

Table 4. Molecular constants of the $X\,^2\Pi$ state employed in the simulation of the PO spectrum. Units of cm^{-1}.

	$X\,^2\Pi$, $v = 0$ (cm^{-1})	
	This study	Verma and Singhal[47]
B	0.73063 ± 0.00056	0.73106 ± 0.00003

A	223.908 ± 0.023	224.01 ± 0.01
γ	0.0909 ± 0.0085	
p	0.0201 ± 0.0015	-0.007
q	-0.00118 ± 0.00023	
D	(1.34 ± 0.36) × 10^{-6}	(1.31 ± 0.05) × 10^{-6}
	$X\,^2\Pi$, v = 1, (cm^{-1})	
	This study	Verma and Singhal[47]
T	1220.173 ± 0.013	1220.22 ± 0.02
B	0.72547 ± 0.00085	0.72551 ± 0.00003
A	223.323 ± 0.026	224.18 ± 0.01
γ	0.119 ± 0.017	
p	0.0215 ± 0.0020	-0.007
q	-0.00397 ± 0.00059	
D	- (1.29 ± 0.91) × 10^{-7}	(1.41 ± 0.05) × 10^{-6}

Table 5. Molecular constants of the $A^2\Sigma^+$ state employed in the simulation of the PO spectrum. Units of cm^{-1}.

	$A^2\Sigma^+$,v = 0 (cm^{-1})	
	This study	Coquart *et al.*[28]
T	40486.613 ± 0.021	40485.61
B	0.77740 ± 0.00055	0.77725
D	(1.23 ± 0.34) × 10^{-6}	1 × 10^{-6}
	$A^2\Sigma^+$, v = 1, (cm^{-1})	
	This study	Coquart *et al.*[28]
T	41863.138 ± 0.013	41862.76
B	0.77251 ± 0.00089	0.77195
D	(1.3 ± 1.0) × 10^{-6}	1 × 10^{-6}

Table 6. Molecular constants of the $^4\Sigma^-$ (v= 4) perturbing level employed in the simulation of the PO spectrum. Units of cm^{-1}.

	$^4\Sigma^-$, v= 4 (cm^{-1})	
	This study	Verma and Singhal[47]
T	40518.77 ± 0.24	40517.69 ± 0.23
B	0.5982 ± 0.0012	0.5984 ± 0.0012
λ_{SS}	0.935 ± 0.066	0.33 ± 0.11
γ	0.0297 ± 0.0069	0.020 ± 0.008
D	0	0.6 × 10^{-6}
$6^{½}$<$^4\Sigma^-$|H|$A^2\Sigma^+$,v = 0>	4.593 ± 0.011	-7.235 ± 0.093

706

707 *4.4 Atmospheric Implications*

708 Interplanetary dust particles entering the upper atmosphere of a terrestrial planet will
709 undergo meteoric ablation at around the 1 μbar pressure region.[56] Phosphorus will ablate
710 from these particles as either PO or PO_2,[7] and these molecules will mostly dissociate to form
711 ground and excited state P atoms following hyperthermal collisions with atmospheric
712 molecules. Peak ablation in the Earth's atmosphere occurs around 85 km,[56] and the P atoms
713 formed in this region will be quickly oxidised by O_2 to PO.[8] These PO molecules will then
714 react with O_2, with an e-folding lifetime of around 2.5 ms. At the low pressure at this altitude
715 ($< 10^{-5}$ bar), the reaction will proceed *via* the 2-body bimolecular channel to form PO_2 and O.
716 As the concentration of O_3 at this altitude is around 10^5 times lower than O_2,[57] removal of
717 PO_2 by O_3 to PO_3 will be a very slow process: if this were the only process removing PO_2, it
718 would have a lifetime of ~ 7.5 days. This suggests PO_3 will not be a major reservoir of
719 meteor ablated P. As there are no exothermic processes to convert PO_2 back to PO, the
720 speciation of phosphorus should essentially depend on the reactions converting PO_2 into
721 HPO_2, HOPO, and $HOPO_2$, as illustrated in Figure 1.

722

723 **5. Conclusions**

724 The reactions of PO with O_2 (R2) and PO_2 with O_3 (R3) have been studied both
725 experimentally and theoretically, with this being the first study to our knowledge of reaction
726 R3. For reaction R2, there are significant discrepancies in the literature values reported for k_2
727 at room temperature, with values varying by around a factor of 60. We have determined with
728 the PLP-LIF technique a rate coefficient at the top end of the literature values, with k_2(294 K)
729 = (1.44 ± 0.11) × 10^{-11} cm^3 $molecule^{-1}$ s^{-1} at P ~ 10 Torr. Rate coefficients for R2 determined
730 over a range of pressures also indicate the presence of a three-body channel, in which PO +
731 O_2 combine to form PO_3 (R2b). The potential energy surfaces of both the PO + O_2 and PO_2 +
732 O_3 systems were determined using electronic structure theory, and these calculations
733 combined with RRKM theory to explain the observed pressure and temperature dependences.
734 For PO + O_2, at pressures typical of a planetary upper atmosphere where meteoric ablation of
735 P will occur, the reaction is effectively pressure independent with a yield of PO_2 + O of >
736 99%, and can be expressed by: $\log_{10}(k_2,\ 120 - 500\ K,\ cm^3\ molecule^{-1}\ s^{-1}) = -13.915 + 2.470\log_{10}(T) - 0.5020(\log_{10}(T))^2$, with an uncertainty of ± 10 % over the experimental
738 temperature range (191 – 339 K). With increasing pressure, the yield of PO_3 increases,
739 reaching ~ 90% at a pressure of 1 atm and T = 300 K. For PO_2 + O_3, $k_3(PO_2 + O_3) = 3.7 \times 10^{-11} \exp^{(-1131/T)}$ cm^3 $molecule^{-1}$ s^{-1}, with an uncertainty of ± 26 % over the experimental
741 temperature range (188 – 339 K). Laser induced fluorescence spectra of PO over the
742 wavelength range of 245 – 248 nm were collected and fitted using the PGOPHER program,
743 which yields new spectroscopic constants for the ground and v = 1 vibrational levels of the X
744 $^2\Pi$ and $A^2\Sigma^+$ states of PO.

745 **Acknowledgements**

This study was supported by funding from the UK Science and Technology Facilities Council (grant ST/P000517/1). The raw and processed data produced by this study is archived at Leeds University and is available upon request to JMCP.

References

1. Maciá, E. The role of phosphorus in chemical evolution. *Chem. Soc. Rev.* **2005,** *34*, 691-701.

2. Lodders, K. Solar system abundances and condensation temperatures of the elements. *Astrophys. J.* **2003,** *591*, 1220-1247.

3. Redfield, A. C. The biological control of chemical factors in the environment. *Am. Sci.* **1958,** *46*, 205-221.

4. Schwartz, A. W. Phosphorus in prebiotic chemistry. *Philos. T. Roy. Soc. B* **2006,** *361*, 1743-1749.

5. Pasek, M. A. Rethinking early Earth phosphorus geochemistry. *P. Natl. A. Sci.* **2008,** *105*, 853-858.

6. Plane, J. M. C.; Flynn, G. J.; Määttänen, A.; Moores, J. E.; Poppe, A. R.; Carrillo-Sanchez, J. D.; Listowski, C. Impacts of cosmic dust on planetary atmospheres and surfaces. *Space Sci. Rev.* **2017,** *214*, 23.

7. Carrillo-Sánchez, J. D.; Bones, D. L.; Douglas, K. M.; Flynn, G. J.; Wirick, S.; Fegley, B.; Araki, T.; Kaulich, B.; Plane, J. M. C. Injection of meteoric phosphorus into planetary atmospheres. *Planet. Space. Sci.* **2020,** *187*, 104926.

8. Douglas, K. M.; Blitz, M. A.; Mangan, T. P.; Plane, J. M. C. Experimental Study of the Removal of Ground- and Excited-State Phosphorus Atoms by Atmospherically Relevant Species. *J. Phys. Chem. A* **2019,** *123*, 9469-9478.

9. Frisch, M. J.; Trucks, G. W.; Schlegel, H. B.; Scuseria, G. E.; Robb, M. A.; Cheeseman, J. R.; Scalmani, G.; Barone, V.; Petersson, G. A.; Nakatsuji, H., et al. *Gaussian 16 Rev. B.01*, Wallingford, CT, 2016.

10. Henshaw, T. L.; MacDonald, M. A.; Stedman, D. H.; Coombe, R. D. The $P(^4S_u)$ + $N_3(^2\Pi_g)$ reaction: chemical generation of a new metastable state of PN. *J. Phys. Chem.* **1987,** *91*, 2838-2842.

11. Clyne, M. A. A.;Ono, Y. Kinetic studies of ground-state phosphorus atoms. *J. Chem. Soc. Farad. T. 2* **1982,** *78*, 1149-1164.

12. Husain, D.;Slater, N. K. H. Time-resolved resonance fluorescence studies of ground state phosphorus atoms, $P[3p^3(^4S_{3/2})]$. *J. Chem. Soc. Farad. T. 2* **1978,** *74*, 1627-1643.

13. Husain, D.;Norris, P. E. Reactions of phosphorus atoms, $P(3^4S_{3/2})$, studied by attenuation of atomic resonance radiation in vacuum ultraviolet. *J. Chem. Soc. Farad. T. 2* **1977,** *73*, 1107-1115.

14. Aleksandrov, E. N.; Arutyunov, V. S.; Dubrovina, I. V.; Kozlov, S. N. On the role of PO radicals in the reaction of phosphorus oxidation. *Dokl. Akad. Nauk. SSSR* **1982,** *267*, 110-113.

15. Wong, K. N.; Anderson, W. R.; Kotlar, A. J.; Dewilde, M. A.; Decker, L. J. Lifetimes and quenching of the B $^2\Sigma^+$ PO by atmospheric gases. *J. Chem. Phys.* **1986,** *84*, 81-90.

16. Long, S. R.; Christesen, S. D.; Force, A. P.; Bernstein, J. S. Rate constant for the reaction of PO radical with oxygen. *J. Chem. Phys.* **1986,** *84*, 5965-5966.

17. Sausa, R. C.; Miziolek, A. W.; Long, S. R. State distributions, quenching, and reaction of the PO radical generated in Excimer laser photofragmentation of dimethyl methylphosphonate. *J. Phys. Chem.* **1986,** *90*, 3994-3998.

18. De Beck, E.; Kaminski, T.; Patel, N. A.; Young, K. H.; Gottlieb, C. A.; Menten, K. M.; Decin, L. PO and PN in the wind of the oxygen-rich AGB star IK Tauri. *Astron. Astrophys.* **2013,** *558*, 9.

19. Tenenbaum, E. D.; Dodd, J. L.; Milam, S. N.; Woolf, N. J.; Ziurys, L. M. Comparatie spectra of oxygen-rich versus carbon-rich circumstellar shells: VY Cannis Majoris and IRC + 10216 at 215-285 GHz. *Astrophys. J. Lett* **2010,** *720*, L102-L107.

20. Ziurys, L. M.; Milam, S. N.; Apponi, A. J.; Woolf, N. J. Chemical complexity in the winds of the oxygen-rich supergiant star VY Canis Majoris. *Nature* **2007,** *447*, 1094-1097.

21. Gobrecht, D.; Cherchneff, I.; Sarangi, A.; Plane, J. M. C.; Bromley, S. T. Dust formation in the oxygen-rich AGB star IK Tauri. *Astron. Astrophys.* **2016,** *585*, A6.

22. Jayaweera, T. M.; Melius, C. F.; Pitz, W. J.; Westbrook, C. K.; Korobeinichev, O. P.; Shvartsberg, V. M.; Shmakov, A. G.; Rybitskaya, I. V.; Curran, H. J. Flame inhibition by phosphorus-containing compounds over a range of equivalence ratios. *Combust. Flame* **2005,** *140*, 103-115.

23. Korobeinichev, O. P.; Shvartsberg, V. M.; Bol'shova, T. A.; Shmakov, A. G.; Knyaz'kov, D. A. Inhibition of methane-oxygen flames by organophosphorus compounds. *Cobust, Explo. Shock Waves* **2002,** *38*, 127-133.

24. MacDonald, M. A.; Jayaweera, T. M.; Fisher, E. M.; Gouldin, F. C. Inhibition of nonpremixed flames by phosphorus-containing compounds. *Combust. Flame* **1999,** *116*, 166-176.

25. Korobeinichev, O. P.; Shvartsberg, V. M.; Shmakov, A. G. The chemistry of combustion of organophosphorus compounds. *Russ. Chem. Rev.* **2007,** *76*, 1021-1047.

26. Zegers, E. J. P.;Fisher, E. M. Gas-phase pyrolysis of diisopropyl methylphosphonate. *Combust. Flame* **1998,** *115*, 230-240.

27. Moussaoui, Y.; Ouamerali, O.; De Mare, G. R. Properties of the phosphorus oxide radical, PO, its cation and anion in their ground electronic states: comparison of theoretical and experimental data. *Int. Rev. Phys. Chem.* **2003,** *22*, 641-675.

28. Coquart, B.; Paz, M. D.; Prudhomme, J. C. Transition $A^2\Sigma^+$–$X^2\ \Pi$ des molécules $P^{16}O$ et $P^{18}O$. Perturbations de l'état $A^2\Sigma^+$. *Can. J. Phys.* **1975,** *53*, 377-384.

29. Wong, K. N.; Anderson, W. R.; Kotlar, A. J. Radiative processes following laser excitation of the A $^2\Sigma^+$ state of PO. *J. Chem. Phys.* **1986,** *85*, 2406-2413.

30. Liu, H.; Shi, D. H.; Sun, J. F.; Zhu, Z. L. Accurate potential energy curves and spectroscopic properties of the 27 Lambda-S states and 73 Omega states of the PO radical. *Mol. Phys.* **2017,** *115*, 714-730.

31. Izzaouihda, S.; El Makarim, H. A.; Komiha, N.; Lahmar, S.; Ghalila, H. Ab-initio potential energy curves of valence and Rydberg electronic states of the PO radical. *Comput. Theor. Chem.* **2014,** *1049*, 102-108.

32. Gómez Martín, J. C.; Blitz, M. A.; Plane, J. M. C. Kinetic studies of atmospherically relevant silicon chemistry Part I: Silicon atom reactions. *Phys. Chem. Chem. Phys.* **2009,** *11*, 671-678.

33. Mangan, T. P.; McAdam, N.; Daly, S. M.; Plane, J. M. C. Kinetic study of Ni and NiO reactions pertinent to the Earth's upper atmosphere. *J. Phys. Chem. A* **2019,** *123*, 601-610.

34. Totterdill, A.; Gómez Martín, J. C.; Kovács, T.; Feng, W.; Plane, J. M. C. Experimental Study of the Mesospheric Removal of NF3 by Neutral Meteoric Metals and Lyman-α Radiation. *J. Phys. Chem. A* **2014,** *118*, 4120-4129.

35. Lewis, T.; Heard, D. E.; Blitz, M. A. A novel multiplex absorption spectrometer for time-resolved studies. *Rev. Sci. Instrum.* **2018,** *89*, 024101.

36. Keller-Rudek, H.; Moortgat, G. K.; Sander, R.; Sörensen, R. The MPI-Mainz UV/VIS Spectral Atlas of Gaseous Molecules of Atmospheric Interest. *Earth Syst. Sci. Data* **2013,** *5*, 365-373.

37. Matsumi, Y.;Kawasaki, M. Photolysis of Atmospheric Ozone in the Ultraviolet Region. *Chem. Rev.* **2003,** *103*, 4767-4782.

38. Hamilton, P. A. The laser-induced fluorescence-spectrum and radiative lifetime of PO_2. *J. Chem. Phys.* **1987,** *86*, 33-41.

39. Hamilton, P. A.;Murrells, T. P. Kinetics and mechanism of the reactions of PH_3 with $O(^3P)$ and $N(^4S)$ atoms. *J. Chem. Soc. Farad. T. 2* **1985,** *81*, 1531-1541.

40. Hamilton, P. A.;Murrells, T. P. Mechanism for the chemiluminescence in oxygen-phosphorus systems. *J. Phys. Chem.* **1986,** *90*, 182-185.

41. Kampf, R. P.;Parson, J. M. Chemiluminescent pathways in reactions of phosphorus, antimony, and bismuth with ozone to form dioxides and monoxides. *J. Chem. Phys.* **1998,** *108*, 7595-7606.

42. Cai, Z. L.; Hirsch, G.; Buenker, R. J. Ab initio study of the electronic spectrum of the PO2 radical. *Chem. Phys. Lett.* **1996,** *255*, 350-356.

43. Ianni, J. C. Kintecus. www.kintecus.com.

44. Glowacki, D. R.; Liang, C. H.; Morley, C.; Pilling, M. J.; Robertson, S. H. MESMER: An open-source master equation solver for multi-energy well reactions. *J. Phys. Chem. A* **2012,** *116*, 9545-9560.

45. Stratmann, R. E.; Scuseria, G. E.; Frisch, M. J. An efficient implementation of time-dependent density-functional theory for the calculation of excitation energies of large molecules. *J. Chem. Phys.* **1998,** *109*, 8218-8224.

46. Frisch, M. J.; Trucks, G. W.; Schlegel, H. B.; Scuseria, G. E.; Robb, M. A.; Cheeseman, J. R.; Scalmani, G.; Barone, V.; Petersson, G. A.; Nakatsuji, H., et al. *Gaussian 16, Revision B.01*, Gaussian, Inc.: Wallingford, CT, USA, 2016.

47. Verma, R. D.;Singhal, S. R. New Results on the $B^2\Sigma^+$, $b^4\Sigma^-$, and $X^2\Pi$ States of PO. *Can. J. Phys.* **1975,** *53*, 411-419.

48. Atkinson, R.; Baulch, D. L.; Cox, R. A.; Crowley, J. N.; Hampson, R. F.; Hynes, R. G.; Jenkin, M. E.; Rossi, M. J.; Troe, J. Evaluated kinetic and photochemical data for atmospheric chemistry: Volume I - gas phase reactions of O-x, HOx, NOx and SOx species. *Atmos. Chem. Phys.* **2004,** *4*, 1461-1738.

49. Montgomery, J. A., Jr. ; Frisch, M. J.; Ochterski, J. W.; Petersson, G. A. A complete basis set model chemistry. VI. Use of density functional geometries and frequencies. *J. Chem. Phys.* **1999,** *110*, 2822-2827.

50. Chase, M. W., Jr.; Davies, C. A.; Downey, J. R., Jr.; Frurip, D. J.; McDonald, R. A.; Syverud, A. N., NIST-JANAF Thermochemical Tables 1985. In *NIST Standard Reference Database 13*, 1998 ed.; Standard Reference Data Program, National Institute of Standards and Technology Gaithersburg, MD, 1998.

51. Gilbert, R. G.;Smith, S. C. *Theory of Unimolecular and Recombination Reactions*. Blackwell: Oxford, 1990.

52. Burkholder, J. B.; Sander, S. P.; Abbatt, J.; Barker, J. R.; Huie, R. E.; Kolb, C. E.; Kurylo, M. J.; Orkin, V. L.; Wilmouth, D. M.; Wine, P. H. Chemical Kinetics and Photochemical Data for Use in Atmospheric Studies, Evaluation No. 18. http://jpldataeval.jpl.nasa.gov.

53. Peiró-García, J.;Nebot-Gil, I. Ab initio study of the mechanism of the atmospheric reaction: NO_2+O_3 -> NO_3 + O_2. *J. Comput. Chem.* **2003,** *24*, 1657-1663.

54. Scuseria, G. E.; Janssen, C. L.; III, H. F. S. An efficient reformulation of the closed-shell coupled cluster single and double excitation (CCSD) equations. *J. Chem. Phys.* **1988,** *89*, 7382-7387.

55. Western, C. M. PGOPHER: A program for simulating rotational, vibrational and electronic spectra. *J. Quant. Spectrosc. Radiat. Transfer* **2017,** *186*, 221-242.

56. Plane, J. M. C.; Feng, W. H.; Martin, J. C. G.; Gerding, M.; Raizada, S. A new model of meteoric calcium in the mesosphere and lower thermosphere. *Atmos. Chem. Phys.* **2018,** *18*, 14799-14811.

57. Plane, J. M. C. Atmospheric chemistry of meteoric metals. *Chem. Rev.* **2003,** *103*, 4963-4984.

910

911 TOC Graphic

912

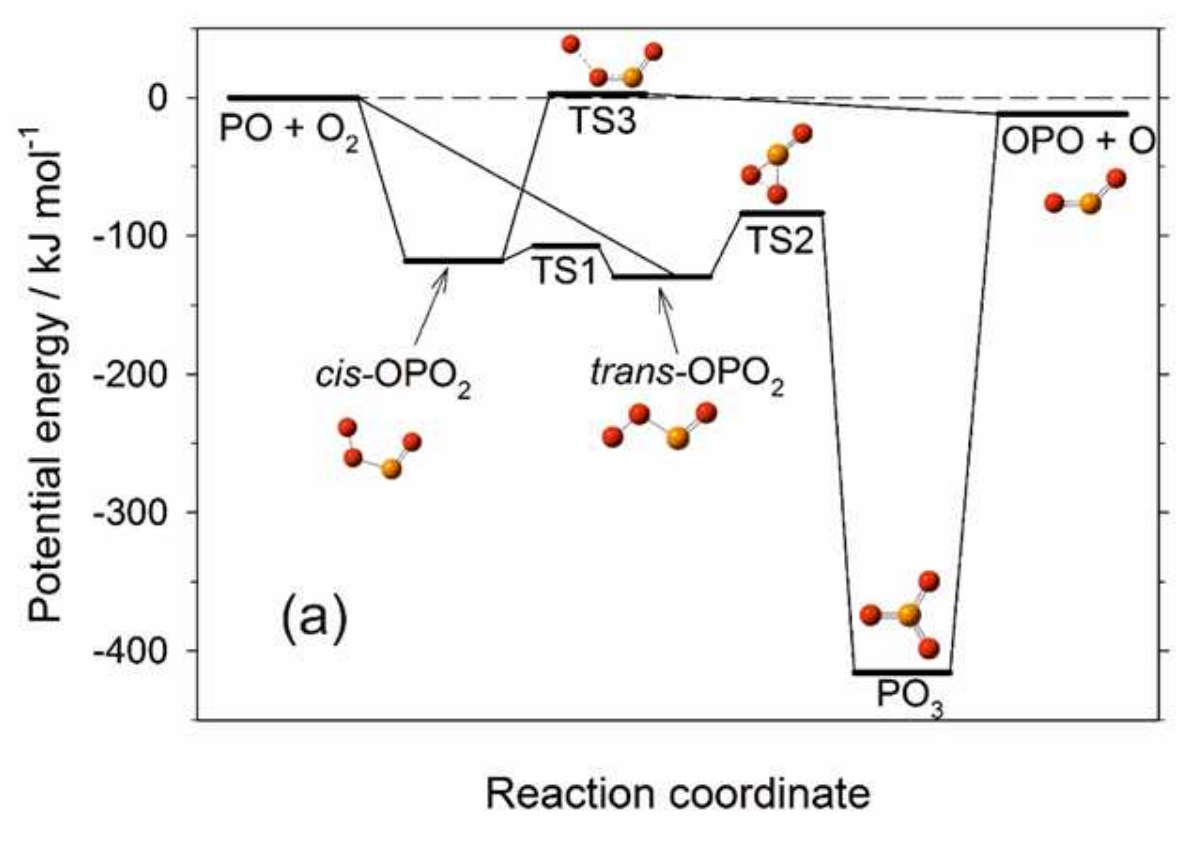

913